Table of Contents

DE GRUYTER

HUNGARIAN JOURNAL OF INDUSTRY AND CHEMISTRY
Vol. 45(2) pp. 1–7 (2017)
hjic.mk.uni-pannon.hu
DOI: 10.1515/hjic-2017-0012

HUNGARIAN JOURNAL OF INDUSTRY AND CHEMISTRY
HJIC

METHYL-*TERT*-BUTYL-ETHER SYNTHESIS REACTOR MODELLING AND OPTIMIZATION USING AN ASPEN CUSTOM MODELER

ZEESHAN NAWAZ

SABIC Technology & Innovation, PO Box 42503, Saudi Basic Industries Corporation (SABIC), Riyadh, 11551, SAUDI ARABIA

A pseudo-homogeneous model of methyl-*tert*-butyl-ether (MTBE) synthesis in a multi-tubular packed-bed reactor has been developed using an Aspen Custom Modeler (ACM) for selecting optimum operating strategies, for the maximization and enhancement of MTBE production, and isobutylene consumption, respectively. The model accounts for mass, energy and momentum balances; and the effectiveness factor is evaluated in a one-dimensional pseudo-homogeneous model. The kinetic investigation contains kinetic rate expressions as given by the effectiveness factor for accounting the resistance of pellets in terms of mass and heat transfer. An activity coefficient can be used in order to systematically obtain a new steady-state solution. The model used literature-based correlations for the estimation of heat transfer coefficients. The value of the coefficient for gas-coolant heat transfer can be adjusted by using a tuning coefficient in order to enrich the process data. Reasonable agreement was found between model predictions and data under similar conditions. The studies concerning model sensitivity compute the optimum temperature, pressure, feed flow rate, methanol/isobutylene ratio, heat removal rate, etc. of the reactor and suggest optimum operating conditions of the reactor.

Keywords: methyl-*tert*-butyl-ether (MTBE) synthesis, lead reactor, multi-tubular packed-bed, Aspen Custom Modeler (ACM), isobutylene

1. Introduction

Methyl-*tert*-butyl-ether (MTBE) is of importance among petrochemicals due to its physicochemical properties and as an additive in gasoline. It contributes to the gradual elimination of lead-based additives, increasing the octane number (as an octane booster) and serves as a volume extender [1]. It is formed by the etherification reaction of an alcohol with a tertiary olefin. Ethers are preferable over alcohols due to their lower sensitivity values, i.e. the difference between the RON (Research Octane Number) and MON (Motor Octane Number) [2]. Today, standard (Huls AG) and Ethermax are the known processes commercialized by Snamprogetti, CDTech, Universal Oil Products (UOP), Axens, Fortum, Arco, Phillips, BP-Intevep, Sinopec, Sumitomo, etc. These are similar processes to each other. In this study a Snamprogetti-lead reactor is modelled to maximize its productivity.

2. Experimental Conditions Considered

2.1. Reaction Chemistry

The following five reactions (*Eqs.(1-5)*) are involved in MTBE synthesis when isobutylene reacts with methanol (MeOH). MTBE synthesis is an exothermic liquid-phase reversible reaction catalysed by a cationic ion-exchange resin (sulphonated macroporous polystyrene). For each mole of isobutylene converted, ~37.7 kJ of heat is released and the thermodynamic equilibrium determines the extent of conversion [1-2].

MTBE: $CH_3OH + (CH_3)_2C{=}CH_2 \leftrightarrow (CH_3)_3COCH_3$ (1)

However, undesirable side reactions may take place such as the dimerization of isobutylene to diisobutenes (DIB), 2,4,4-trimethyl-1-pentene (TMP-1) and 2,4,4-trimethyl-2-pentene (TMP-2); and the formation of methyl sec-butyl ether (MSBE), dimethyl ether (DME) and tert-butyl alcohol (TBA). The water produced during the formation of DME may react with isobutylene to form tert-butyl alcohol (TBA) and its blending octane number is lower than that of MTBE. On the other hand, the presence of water reduces the acidity of the catalyst (reducing activity) and therefore a higher reaction temperature is required.

DIB: $2\,(CH_3)_2C{=}CH_2 \leftrightarrow (CH_3)_3CH_2(CH_3)C{=}CH_2 + (CH_3)_3C(H){=}C(CH_3)_2$ (2)

MSBE: $CH_3OH + (C_2H_5)CH{=}CH_2 \leftrightarrow CH_3CH(OCH_3)(CH_2CH_3)$ (3)

DME: $2\,CH_3OH \leftrightarrow CH_3OCH_3 + H_2O$ (4)

TBA: $(CH_3)_2C{=}CH_2 + H_2O \leftrightarrow (CH_3)_3COH$ (5)

*Correspondence: zeeshan@sabic.com

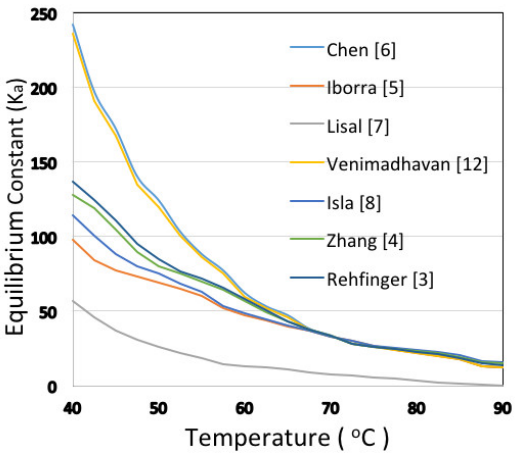

Figure 1. Values of the equilibrium constant K_a as a function of temperature.

2.2. Thermodynamics

Etherification is an exothermic equilibrium reaction between a primary alcohol and an *iso*-olefin containing a double bond on a tertiary carbon atom (such as isobutene (iBu) under the operating temperature and pressure. Owing to the non-ideality of liquid mixtures due to their disparate polarities and equilibria, the kinetic rate expressions for the synthesis of MTBE are generally given in terms of component activities. Equilibrium and rate equations based on activities were first proposed by Rehfinger *et al.* [3] and kinetic (including the effectiveness factor) and equilibrium data from an isothermal packed-bed reactor using the catalyst Amberlyst-15 were discussed by Zhang *et al.* [4]. The activity-based equilibrium constant is expressed as:

$$K_a = \left[\frac{a_{\mathrm{MTBE}}}{a_{\mathrm{iBu}} \cdot a_{\mathrm{MeOH}}}\right]_{\mathrm{eq.}} = \left[\frac{\gamma_{\mathrm{MTBE}}}{\gamma_{\mathrm{iBu}} \cdot \gamma_{\mathrm{MeOH}}} \cdot \frac{x_{\mathrm{MTBE}}}{x_{\mathrm{iBu}} \cdot x_{\mathrm{MeOH}}}\right]_{\mathrm{eq.}} \quad (6)$$

where a_{MeOH}, a_{iBu}, and a_{MTBE} are the activities of methanol, isobutene, and MTBE, respectively, while γ and x are the activity coefficients and mole fractions of these components, respectively.

The values of the equilibrium constant (K_a) published in the literature vary significantly (*Fig.1*) as a function of temperature [3-10]. Deviations may stem from the different bases used for the evaluation of the activity coefficient as well as from the operating temperature of the reactor, for example, employing primary reactors or reactive distillation columns.

2.3. Catalysis and Kinetics

The acidic cation exchange macroporous resin catalysts used commercially for the synthesis of MTBE are provided by Bayer, Dow Chemical (Rohm & Haas), Purolite, Kairui, etc. The resins are prepared by the suspension of styrene in the presence of an appropriate cross-linking agent (divinylbenzene (DVB)) for polymerization functionalized by means of sulphonation with sulphuric or chlorosulphonic acid [11]. A reduction in volume of ~20-30% is observed because of the shift of the resin from the hydrated form (as it is generally charged in water) to a more contracted form due to a much less polar-reacting medium (a hydrocarbon/methanol mixture). The usability of the catalyst largely depends upon the process conditions, namely the type of reactor, e.g. a reactor receiving thermal support is better than adiabatic and thermal degradation with breakage of the carbon-sulphur bond (therefore, temperatures below 130 °C are recommended) and feed impurities (cations, e.g. Na, Ca, Fe, Al, Cr, Si, etc., strong N-bases like ammonia and amines, weak N-bases like acetonitrile and propionitrile, and dienes).

Table 1. Properties of the catalyst Amberlyst-15.

Properties	Specifications
Porosity of Catalyst (ε_p)	0.31-0.39
Tortuosity of Catalyst (t)	0.7-1.7
Density of catalyst (kg m^{-3})	~2000
Physical Shape	spherical beads
Ionic Form	hydrogen
Moisture Content (g/g %)	~50
Particle Size (mm)	0.3-1.5
Functional Group	RSO_3H
Surface Area (m^2 g^{-1})	~45
Pore Diameter (Å)	~250
Acid Sites (eq(H^+) kg^{-1})	4.6-5.2

The rate expressions, essential kinetic parameters and thermodynamic data such as the activation energy, effectiveness of the catalyst, heat of reaction, equilibrium constant and so forth have been selected from the literature [3-14]. The rate of reaction depends substantially on two parameters: acidity (type and number of acidic sites) and accessibility (porosity, content, particle diameter and treating medium). In the homogeneous model (in the absence of the diffusion phenomena), the reaction rate can be described in terms of confined catalyst pores, where the reactant concentration is in a partition equilibrium with the corresponding concentrations in the external solution. The rate-determining step was estimated to be the surface reaction between protonated adsorbed methanol and isobutylene [3-13]. This simplifies the rate of consumption for isobutylene after assuming that polar methanol molecules are preferentially adsorbed onto the ion-exchange resin catalyst (*Table 1*) and the fraction of unoccupied sites over the catalyst surface was small as follows [4]:

$$-r_{\mathrm{iBu}} = a_0 \cdot e^{-\frac{E_a}{RT}} \cdot \left(\frac{a_{\mathrm{iBu}}}{a_{\mathrm{MeOH}}} - \frac{1}{K_a} \cdot \frac{a_{\mathrm{MTBE}}}{a^2_{\mathrm{MeOH}}}\right) \quad (7)$$

where r_{iBu} is the rate constant of the reaction, R is the universal gas constant, E_a is the activation energy of 85.4 kJ mol^{-1} (for Amberlyst-15 this value varies between 71 and 93 kJ mol^{-1} and is influenced by not

Table 2. Specifications of the reactor system.

Specification	Units	Value
Reactor Length	m	~8
Reactor Diameter	m	~3.5
LHSV	h^{-1}	~2-9
Porosity	-	~0.35
Feed Inlet Temperature	°C	~40
i-C_4/MeOH Ratio	molar	~1.1
Pressure	bar	~10
Recycling Ratio	%	~15

only the type of catalyst but also by the composition of the reaction mixture); and $a_0 = 6.3 \times 10^{12}$ mol h^{-1} g^{-1}.

The effective diffusion coefficient and activation energy of methanol over Amberlyst-15 at 60 °C was estimated to be $2.3 \cdot 10^{-9}$ m^2 s^{-1} and ~35.4 kJ mol^{-1}, respectively [4]. The given value of the effective diffusion coefficient is slightly lower than the one Rehfinger and Hoffmann reported ($3.5 \cdot 10^{-9}$ m^2 s^{-1}) [3]. The catalysts Kastel CS 381 and Amberlyst CSP used in the synthesis of MTBE possess similar rate constants to Amberlyst-15, whereas Amberlyst XE 307 and Duolite ES 276 have significantly higher; and Duolite C16P and Duolite C26 have substantially lower values for their rate constants [3-15]. Every resin undergoes deactivation, if sodium ions are exchanged for their protons. Due to the acidic nature of resins, the activity is strongly reduced by the presence of basic substances and/or salts in the reaction mixture. The heat of reaction, $\Delta H°$(MTBE), in the liquid phase at 25 °C was reviewed by Iborra *et al.* and found to be within the range of -34 to -40 kJ mol^{-1} [5].

The rate for dimerization of isobutene (DIB formation) [4, 10] can be calculated as follows:

$$r_{\mathrm{DIB}} = k_0 \cdot e^{\frac{-66.7\,\mathrm{kJ/mol}}{R}\cdot\left(\frac{1}{T}-\frac{1}{333}\right)} \cdot \frac{a_{\mathrm{iBu}}^2}{K_{\mathrm{ad}} \cdot a_{\mathrm{MeOH}} + a_{\mathrm{iBu}}} \quad (8)$$

where the unit of r_{DIB} is mmol s^{-1} eq^{-1}, K_{ad} is the ratio of adsorption equilibrium constants, and k_0 is the frequency factor of the kinetic constant.

2.4. Reactor and Process

Generally, the multi-tubular packed-bed reactor is used exclusively as a front-end for the reactor performing the synthesis of MTBE, where the catalyst is lodged in the tubes (~10,000 tubes of diameter ~30 mm, length ~6 m, $\varepsilon = 0.4$). The cooling water flows in the shell side and can either flow co- or counter-current. The reactor column is used solely for finishing and exploits the principle of catalytic distillation possessing the normal fractionation trays with reactive trays (where the catalyst is packed) [2, 16]. Therefore, the maximum degree of isobutene conversion was achieved and reactants were separated from the product simultaneously, as MTBE has a much higher boiling temperature. Reactor parameters used for the modelling are given in *Table 2*. Almost all the commercial etherification technologies use similar sections with regard to operation and separation, but are different in terms of type of reactors, numbers and process schemes [16-17]. The MTBE plant consists of a multi-tubular packed-bed reactor, and reactive distillation and methanol recovery sections. There are two separation towers after each reactor that recover the C_4/methanol azeotrope from the top and MTBE from the bottom, followed by the washing tower where water removes the methanol from the C_4, and then a distillation tower to separate water and methanol.

3. Reactor Modelling

Classical models of multi-tubular packed-bed reactors (pseudo-homogeneous one-dimensional) have been extensively discussed in the literature [1, 3-5]. In this study, a custom model of an MTBE water-cooled multi-tubular packed-bed reactor was built using an Aspen-based platform (ACM) with the ultimate objective of developing a complete process flow-sheet using the same method as in Refs. [18-19]. Model equations have been developed based on the following assumptions:

- steady-state operation;
- plug flow with no axial mixing;
- one dimensional as no temperature and composition gradients exist in a radial direction (perfect radial mixing);
- pseudo-homogeneous conditions for fluid - solid phase interactions: transport limitations in terms of catalyst particles are taken into account by using the concept of an effectiveness factor;
- heat transfer coefficient of the liquid phase to coolant (constant value along the reactor axis) is implemented as a sub-model. The heat transfer coefficient was evaluated under various changeable process parameters as defined the coolant inlet temperature, inlet flow rate, inlet pressure and inlet composition;
- pressure drops according to the Ergun equation in the model.

3.1. Mass and Energy Balance

The steady-state material balance in the liquid phase expressed in terms of vectors of the molar flow rates of the components in z direction is

$$\frac{\mathrm{d}\mathbf{f}}{\mathrm{d}z} = A\mathbf{r} \quad \text{and} \quad \mathbf{r} = \rho_{\mathrm{b}} \cdot \mathbf{S}^{\mathrm{T}} \cdot \mathbf{r}_{\mathrm{kef}} \quad (9)$$

where $\mathbf{r}$ is the vector of the rate of production or consumption per unit volume of a component, $\mathbf{S}$ is the stoichiometric matrix, $\mathbf{r}_{\mathrm{kef}}$ is the vector of effective reaction rates, A is the cross-sectional area of the reactor, $\mathbf{f}$ is a molar flow rate vector of the component, and ρ_{b} the bulk density of the catalyst.

The liquid side of the heat balance equation under steady-state conditions is as follows:

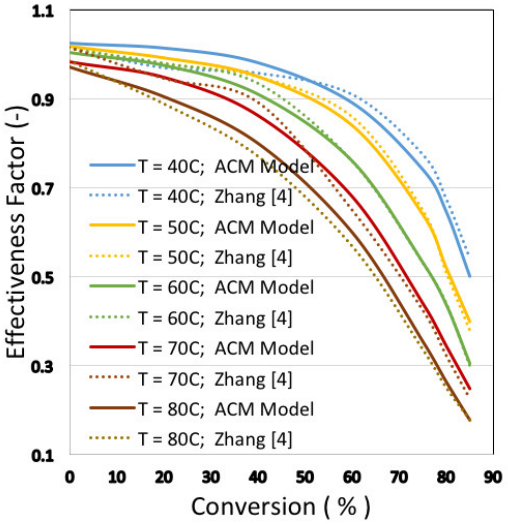

Figure 2. Effectiveness factor for the MTBE synthesis reaction based on data from Ref. [4].

$$\frac{dT}{dz} = \frac{\left|\left(\Delta \mathbf{h}_R\right)^T \cdot \boldsymbol{r}_{kef}\right| A - h_{fc}\,\pi D_t \left(T - T_c\right)}{\mathbf{f}^T \cdot \mathbf{c}_p} \qquad (10)$$

where $\Delta\mathbf{h}_R$ is the vector concerning the heat of reaction, $\mathbf{c}_p$ is the vector concerning the molar specific heat of a component, T and T_c are the liquid phase and coolant absolute temperatures, respectively, h_{fc} is the liquid-to-coolant heat transfer coefficient, and D_t is the diameter of the reactor tube.

The shell side of the heat balance equation under steady-state conditions is as follows:

$$\frac{dT_c}{dz} = \pm \frac{h_{fc} \cdot \pi \cdot D_t \left(T - T_c\right)}{F_{Vcool} \cdot \rho_{cool} \cdot c_{s,cool}} \qquad (11)$$

where F_{Vcool} is the volumetric flow rate of the coolant, ρ_{cool} is the density of the coolant, and $c_{s,cool}$ is the specific heat capacity of the coolant. In terms of modelling, the negative sign stands for the counter-current and the positive sign for the co-current.

The boundary conditions at the inlet of the reactor in terms of the material and energy balance differential equations are $z = 0$, $F_i(0) = F_{0,i}$, $T(0) = T_0$, $T_c(0) = T_{cool,in}$ and $T_c(R_L) = T_{cool,in}$.

3.2. Effectiveness Factor

The effectiveness factor for the synthesis of MTBE has been evaluated on the basis of data concerning the generalized Thiele modulus (ϕ_g) [3]:

$$\eta = \tanh(\underline{\phi}_g) / \underline{\phi}_g \,. \qquad (12)$$

In terms of the pseudo-homogeneous model, the effectiveness factor is expressed as a function of temperature and conversion:

$$\eta = \frac{1}{x_1 \cdot e^{\frac{-x_2}{RT}} \cdot \left(1.1 - \left(\frac{\text{conversion \%}}{100}\right)^{x_3} + x_4\right)} \,. \qquad (13)$$

The parameters x_1 – x_4 have been evaluated by minimizing the absolute error between evaluations by Zhang *et al.* [4] and the values predicted by *Eq. 13*. The accuracy of the prediction is shown in *Fig.2*.

3.3. Overall Heat Transfer Coefficient

The overall heat transfer coefficient, taking into account the small value of the wall thickness, is evaluated as follows:

$$h_{fc} = \frac{1}{\left[\frac{1}{h_{fw}} + \frac{D_{te} - D_{ti}}{2 \cdot \lambda_{pipe}} + r_{fouling} + \frac{1}{h_{shell}}\right]} \qquad (14)$$

where D_{ti} and D_{te} are the internal and external diameters of the reactor tube, respectively, λ_{pipe} is the thermal conductivity of the reactor tube, h_{fw} is the fluid-to-wall heat transfer coefficient, h_{shell} is the shell side (wall-to-cooling water) heat transfer coefficient, and $r_{fouling}$ is the fouling factor.

The evaluation of the fluid-to-wall heat transfer coefficient was conducted on the basis of a newly proposed correlation for the estimation of the total (wall and effective thermal conductivity effects) heat transfer coefficient [16]:

$$\mathrm{Nu_f} = \left[3.87 - 3.77 \cdot \exp\left(\frac{-1.37}{D_{ti}/d_p}\right) \cdot \mathrm{Re_f}^{0.643} \cdot \mathrm{Pr_f}^{0.333}\right] . \qquad (15)$$

In this case, both $\mathrm{Nu_f}$ and $\mathrm{Re_f}$ are expressed based on particle diameters. The heat transfer coefficient of the shell side is expressed as a function of Nu and Re and are both based on the external diameter of the tube, where ε_φ stands for a correction factor accounting for the angle between the coolant stream and reactor tubes:

$$\mathrm{Nu_s} = 0.4 \cdot \varepsilon_\phi \cdot \mathrm{Re_s}^{0.6} \cdot \mathrm{Pr_s}^{0.333} \,. \qquad (16)$$

3.4. ACM Property Estimations

The physical properties of components and mixtures like viscosity, density and specific heat, were estimated by Aspen Properties (using UNIFAC - Dortmund property package). The ".appdf" file prepared by Aspen Properties is the one called in ACM for seamless transfer of properties. The kinetic sub-model helps in terms of the calculation of reaction heats using the Aspen Properties database.

Table 3. Typical base-case operating conditions and results for the primary reactor.

Specification	Units	Value
tube length	m	6
tube diameter (ID)	mm	21
number of tubes	-	10,000
porosity	-	0.33
feed inlet temperature	ºC	50
isobutene/MeOH ratio	molar	1.1
pressure	bar	8
coolant inlet temperature	ºC	45
feed flow rate	kmol h^{-1}	2,000
isobutene mole fraction	-	0.35
ΔP	bar	0.723
conversion	%	84.7
MTBE selectivity	%	97.86

3.5. Performance Parameters

Reactor performance is evaluated by the following equations:

$$\text{Conversion}(z) = \frac{F_0^{\text{key\_reactant}} - F_z^{\text{key\_reactant}}}{F_0^{\text{key\_reactant}}} \quad (17)$$

$$\text{Selectivity}(z) = \frac{F_z^{\text{key\_product}} - F_0^{\text{key\_product}}}{F_0^{\text{key\_reactant}} - F_z^{\text{key\_reactant}}} \quad (18)$$

$$\text{Yield}(z) = \text{Conversion}(z) \cdot \text{Selectivity}(z) \quad (19)$$

where z stands for the axial coordinate.

4. Model Predictions and Analysis

ACM is the preferred choice for robust reactor modelling. Its equation-oriented modelling platform can be easily exported to Aspen Plus process flow-sheets. The coding of a multi-tubular packed-bed reactor in terms of the synthesis of MTBE was conducted in a modular form. The main reactor model defines the constitutive equations in the bulk phase and sub-models

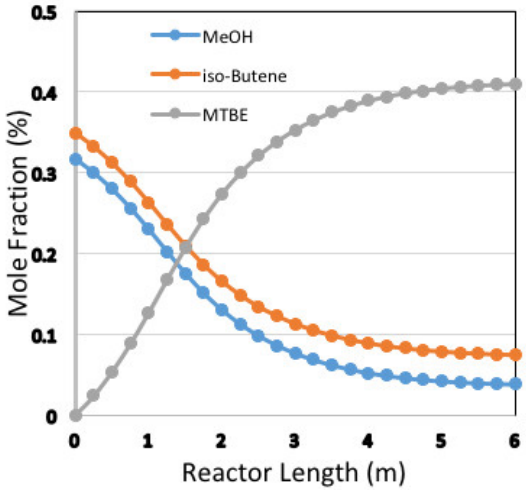

Figure 3. Molar concentration profile along the length of the reactor.

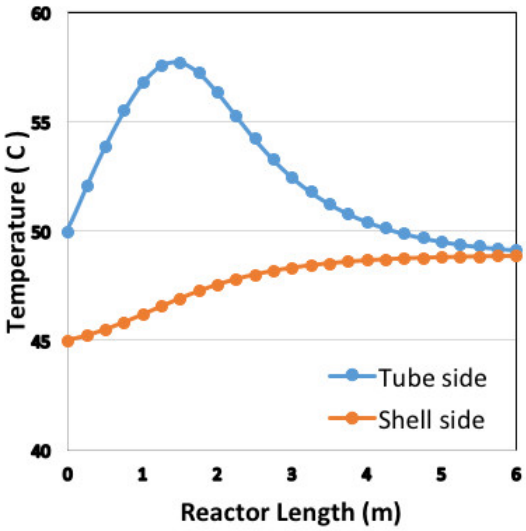

Figure 4. Temperature profiles of the reactor and coolant.

in terms of the reaction kinetics, the estimation of the heat transfer coefficient, and the development of the pellet design. The normal operating conditions for the primary reactor were selected as the base case in terms of modelling (*Table 3*), where MTBE productivity is ~50 T h^{-1}. The molar concentration profile of the reactants and product along the axis of the reactor is shown in *Fig.3*. The full length of the reactor is used for the synthesis of MTBE. *Fig.4* shows the temperature profiles of the reactor and coolant.

The temperature sensitivity is controlled by keeping the temperature difference between the coolant and feed temperatures constant (*Fig.5*). It was observed that due to the exothermic nature of the reaction, the maximum temperature increased significantly with the

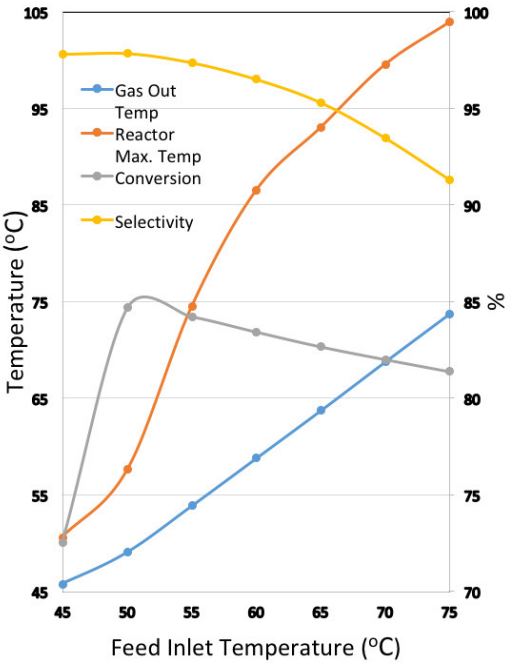

Figure 5. Temperature sensitivity by varying the feed temperature and keeping constant the temperature difference between the coolant and feed temperatures.

Table 4. Dependence of conversion (%), selectivity (%) and the maximum temperature of the reactor (T_{max}) on the isobutene/methanol molar ratio (iBu/MeOH).

iBu/MeOH	0.8	0.9	1.0	1.1	1.2	1.3
conversion	84.7	85.4	85.5	84.6	80.7	76.7
selectivity	98.1	98.1	98.1	97.9	97.1	95.4
T_{max}, ºC	56.1	56.5	56.9	57.7	59.5	62.0

increase in reaction temperature. At a constant pressure and feed flow rate, the increase in the reaction temperature led to an outer mass transfer limitation that strongly affects the rate of conversion. At the same time the selectivity also decreased due to a significant increase in the maximum temperature of the reactor (product degradation) and the maximum rate of conversion was achieved in almost ~30% of the reactor. The isobutylene/methanol molar ratio is one of the key operating parameters and is always kept higher than its stoichiometric value. *Table 4* shows that by deviating from the stoichiometric ratio the effect on the rate of conversion and selectivity also decreases with the increase in the isobutylene/methanol molar ratio.

The predictions according to reactor modelling were found to be in good agreement with data from the literature. The reaction must reach an equilibrium at the rear end of the lead reactor. The estimated effectiveness factor is 0.75 which was also used in the model. The possible explanation for the occurrence of minor discrepancies could be the use of a different catalyst or errors in terms of experimental measurements. It was observed that the maximum degree of productivity corresponded to an isobutene/MeOH molar ratio of close to 1 and a feed inlet temperature of between 50 and 55 ºC. However, it is necessary to synchronize this with the secondary reactor and other unit operations.

5. Conclusion

An ACM-based pseudo-homogeneous model with regard to the synthesis of MTBE using an industrial multi-tubular packed-bed (methyl-*tert*-butyl-ether) reactor has been developed for enhancing operation strategies. The UNIFAC - Dortmund property package was used for reactor modelling. The effectiveness factor was implemented as a function of the reaction temperature. The model was validated using data from the literature. Various sensitivity evaluations were conducted to determine the operational optimization and maximization of MTBE production under different operating parameters. The model was able to predict reaction behaviour and produce temperature and concentration profiles along the length of the reactor. Sensitivity studies were able to calculate the optimum temperature, feed flow rate, methanol/isobutylene ratio as well as heat removal rate of the reactor and thus provide insights into a reasonable operational strategy.

SYMBOLS

A	cross-sectional area of the reactor
a	activity
a_{MeOH}, a_{iBu}, a_{MTBE}, a_{inert}	activities of methanol, isobutene, MTBE and inert isobutane, respectively
a_0	6.3 x 10^{12} mol h^{-1} g^{-1}
$\mathbf{c}_p$	molar specific heat vector of a component
$c_{s,cool}$	specific heat capacity of the coolant
D_t	diameter of the reactor tube
D_{ti}, D_{te}	internal and external diameters of the reactor tube, respectively
E_a	activation energy in kJ mol^{-1}
F_{Vcool}	volumetric flow rate of the coolant
$\mathbf{f}$	molar flow rate vector of a component
h_{fc}	liquid-to-coolant heat transfer coefficient
h_{fw}	fluid-to-wall heat transfer coefficient
h_{shell}	shell side (wall-to-cooling water) heat transfer coefficient
$\Delta\mathbf{h}_R$	heat of reaction vector
γ	activity coefficient
K_a	equilibrium constant (based on activities)
K_{ad}	ratio of adsorption equilibrium constants
K_{MeOH}, K_{iBu}, K_{MTBE}, K_{inert}	adsorption equilibrium constants for methanol, isobutene, MTBE and inert isobutane, respectively
k_0	frequency factor of the kinetic constant
k_r	reaction rate constant
λ_{pipe}	thermal conductivity of the reactor tube
R	universal gas constant
$\mathbf{r}$	vector of the rate of production or consumption per unit volume of a component
$\mathbf{r}_{kef}$	vector of effective reaction rates
$r_{fouling}$	fouling factor
ρ_b	bulk density of the catalyst
ρ_{cool}	density of the coolant
$\mathbf{S}$	stoichiometric matrix
T , T_c	absolute temperatures of the liquid phase and coolant, respectively
x	mole fraction

Acknowledgement

The author gratefully acknowledges the technical support of Prof. Dr. Ing. Teodor Todinca at the University Politechenica Timisoara in Romania.

REFERENCES

[1] Nawaz, Z.: Light alkane dehydrogenation to light olefin technologies: A comprehensive review, *Rev. Chem. Engng.*, 2015 **31**(5), 413–436 DOI 10.1515/revce-2015-0012

[2] DiGirolamo, M.; Sanfilippo, D.: Etherification: Process to improve the quality of distillates, in Beccari M.; Romano, U.; eds. Encyclopaedia of hydrocarbons (ENI S.p.A and Istituto della Enciclopedia Italiana fondata da Giovanni Treccani S.p.A, Roma, Italy) 2006 Vol. II. pp. 193–209

[3] Rehfinger, A.; Hoffmann, U.: Kinetics of MTBE liquid phase synthesis catalyzed by ion-exchange resin. I. Intrinsic rate expression in liquid phase activities, *Chem. Eng. Sci.*, 1990 **45**(6), 1605–1617 DOI 10.1016/0009-2509(90)80014-6

[4] Zhang, T.; Datta, R.: Integral analysis of MTBE synthesis kinetics, *Ind. Eng. Chem. Res.*, 1995 **34**, 730–740 DOI 10.1021/ie00042a004

[5] Iborra, M.; Tejero, J.; Ben El-Fassi, M.; Cunill, F.; Izquierdo, J.F.; Fite, C.: Experimental study of the liquid phase simultaneous synthesis of MTBE and TBA, *Ind. Eng. Chem. Res.*, 2002 **41**, 5359–5365 DOI 10.1021/ie010640q

[6] Chen, F.; Huss, R.S.; Doherty, M.F.; Malone, M.F.: Multiple steady-states in reactive distillation: kinetic effects, *Comp. Chem. Engng.*, 2002 **26**, 81–93 DOI 10.1016/S0098-1354(01)00750-5

[7] Lisal, M.; Smith, W.R.; Nezbeda, I.: Molecular simulation of multicomponent reaction and phase equilibria in MTBE ternary system, *AIChE J.*, 2000 **46**(4), 867–875 DOI 10.1002/aic.690460419

[8] Isla, M.; Irazoqui, H.: Modeling, analysis and simulation of MTBE reactive distillation column, *Ind. Eng. Chem. Res.*, 1996 **35**, 2696–2708 DOI 10.1021/ie9505930

[9] Venimadhavan, G.; Malone, M.F.; Doherty, M.F.: Bifurcation study of kinetic effects in reactive distillation, *AIChE J.*, 1999 **45**(3), 546–556 DOI 10.1002/aic.690450311

[10] Oktar, N.; Murtezaoglu, K.; Dogu, T.; Dogu, G.: Dynamic analysis of adsorption equilibrium and rate parameters of reactants and products in MTBE, ETBE and TAME production, *Can. J. Chem. Eng.*, 1999 **77**, 406–412 DOI 10.1002/cjce.5450770229

[11] Girolamo, M.; Tagliabue, L.: MTBE and alkylate co-production: fundamentals and operating experience, *Catal. Today*, 1999 **52**, 307–319 DOI 10.1016/S0920-5861(99)00084-X

[12] Ancilotti, F.; Fattore, V.: Oxygenate fuels: Market expansion and catalytic aspect of synthesis, *Fuel Proc. Technol.*, 1998 **57**, 163-194 DOI 10.1016/S0378-3820(98)00081-2

[13] Girolamo, M.; Lami, M.; Marchionna, M.; Pescarollo, E.; Tagliabue, L.; Ancilotti, F.: Liquid phase etherification/dimerization of isobutene over sulfonic acid resins, *Ind. Eng. Chem. Res.*, 1997 **36**, 4452–4458 DOI 10.1021/ie9700932

[14] Miracca, I.; Tagliabue, L.; Trotta, R.: Multitubular reactors for etherifications, *Chem. Engng. Science*, 1996 **51**, 2349–2358 DOI 10.1016/0009-2509(96)00091-7

[15] Panneman, H.J.; Beenackers, A.: Influence of the isobutene/methanol ratio and of the MTBE content on the reaction rate of the synthesis of MTBE, *Ind. Eng. Chem. Res.*, 1995 **34**, 3817–3825 DOI 10.1021/ie00038a019

[16] Mariani, N.J.; Martinez, O.M.; Barreto, G.F.: Evaluation of heat transfer parameters in packed beds with cocurrent downflow of liquid and gas, *Chem. Engng. Science*, 2001 **56**, 5995–6001 DOI 10.1016/S0009-2509(01)00225-1

[17] Elkanzi, E.M.: Optimization of MTBE synthesis in a packed-bed reactor system, *Chem. Engng. Proc.*, 1996 **35**, 131–139 DOI 10.1016/0255-2701(95)04122-2

[18] Nawaz, Z.: Dynamic modeling of CATOFIN® packed-bed isobutane dehydrogenation reactor for operational optimization, *Int. J. Chem. Reactor Engng.*, 2016 **14**(1), 491–515 DOI 10.1515/ijcre-2015-0087

[19] Nawaz, Z.: Heterogeneous reactor modeling of an industrial multitubular packed-bed ethylene oxide reactor, *Chem. Engng. Technol.*, 2016 **39**(10), 1845–1857 DOI 10.1002/ceat.201500603

DE GRUYTER

HUNGARIAN JOURNAL OF
INDUSTRY AND CHEMISTRY
Vol. 45(2) pp. 9–12 (2017)
hjic.mk.uni-pannon.hu
DOI: 10.1515/hjic-2017-0013

HUNGARIAN JOURNAL OF INDUSTRY AND CHEMISTRY
HJIC

MODELLING THE PARTIAL DEMINERALIZATION PROCESS OF COW MILK BY SUPERPRO DESIGNER

ATTILA CSIGHY,* ANDRÁS KORIS, AND GYULA VATAI

Department of Food Engineering, Szent István University, Ménesi út 44, Budapest, 1118, HUNGARY

Milk and dairy products contain a number of biologically active compounds (proteins, lipids, vitamins and minerals) that are essential for human nutrition. The most common procedures for demineralization are based on ion exchange-, nanofiltration- and electrodialysis-based technologies. In this study, the application of membrane filtration-based partial demineralization of cow milk was investigated and the process modelled. Using design equations, the partial demineralization process was designed and the economy of the process calculated. The modelling and simulation of the partial demineralization process was carried out by the SuperPro Designer programme. As the first step the unit operations of the demineralization technology were defined using the tools of the programme. The SuperPro Designer possesses industrial tools with reactor models, chemical components, a database of mixtures, and price estimations. By analysing the influence of the operation parameters, the feasibility of the proposed process was investigated. From the results of the modelling it can be concluded that the partial demineralization process can be successfully implemented, achieving the expected demineralization rates with a relatively good payback time of two years.

Keywords: partial demineralization, SuperPro Designer, modelling, economic analysis

1. Introduction

Dairy products play an important role in the health of humans as milk contains a number of biologically active compounds (proteins, lipids, vitamins and minerals). Therefore, the consumption of milk and dairy products is highly recommended [1-2]. Milk is the main raw material in the cheese and casein industry. The disposal of whey creates a major environmental problem for the cheese industry due to the high amount of organic compounds it contains. In the cheese industry to manufacture 1 kg of cheese, 9 kg of whey is produced as a by-product. Whey possesses a large 'biochemical oxygen demand' (BOD) value, therefore, treatment is required before it is released into the environment or recycled. Suárez [3] observed that the nanofiltration membrane is an effective medium for the demineralization of whey. The demineralization efficiency depends on the transmembrane pressure and the volume concentration ratio (VCR). Experimentally, monovalent ions exhibit the highest degree of permeation. [3]

Whey is a watery, dilute liquid, which generally contains 0.8-1.0% total protein, 4.5-5.0% lactose, 0.5-0.7% minerals and 93-94% water. Whey can be divided into two different compositions, namely sweet and acid whey [4]. Another process as part of the treatment of whey is demineralization. Upon demineralization, whey can be used for manufacturing drinks, desserts or ice-cream products. A novel alternative process for demineralization is nanofiltration. Nanofiltration is a membrane separation method that lies between ultrafiltration and reverse osmosis. Nanofiltration membranes can maintain monovalent ions (NaCl) and also organic compounds between 300 and 100 in the Dalton range. Nanofiltration is an effective technique to remove salts, while preserving valuable components [5].

In order to examine the feasibility of the process, technological and economic experiments were carried out by the SuperPro Designer software [6]. This programme is widely used in the pharmaceutical, biotechnology and food industries. The SuperPro Designer is capable of preparing technological and economic documentations and reports about the modelled process. The programme possesses an industrial tool, where the unit operations (reactions, solid/liquid separation, tanks) can be prepared [7]. The purpose of this study is to model the demineralization process using the SuperPro Designer programme and by analyzing the influence of the operation parameters, the feasibility of the proposed process was investigated.

2. Experimental

2.1. Materials and Methods

In this study, one ultrafiltration (UF) and two nanofiltration (NF) membranes were used. The first step was the pre-concentration of milk using the UF

*Correspondence: csighy.attila@gmail.com

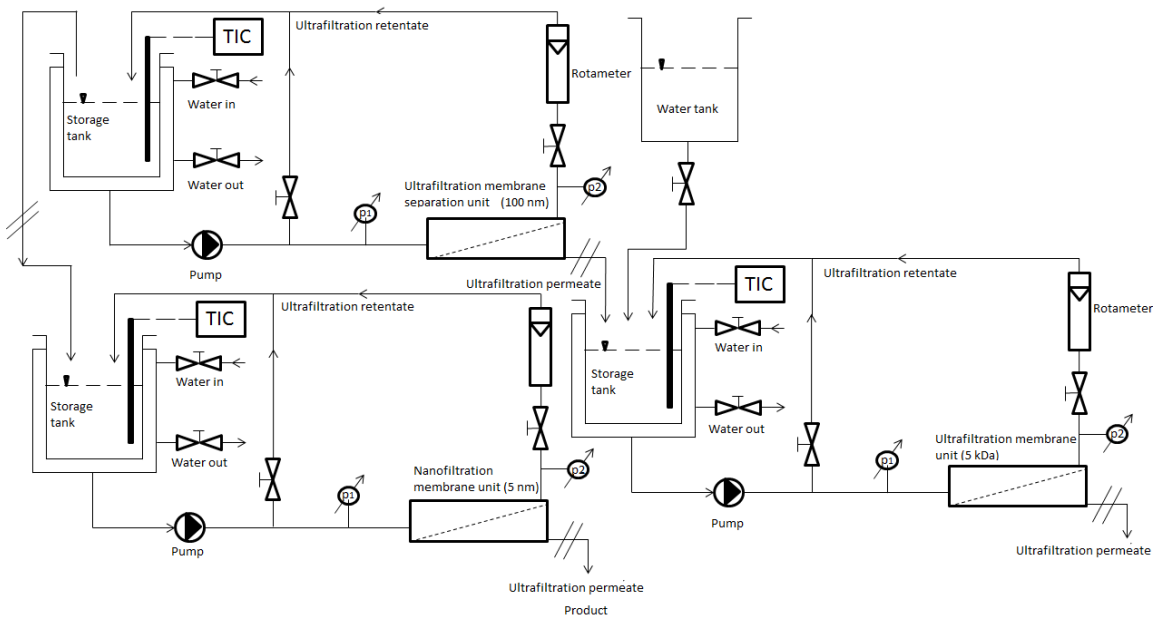

Figure 1. Process flow diagram of the demineralization of cow milk.

membrane. A Schumasiv type 100 nm pore size membrane was used for the pre-concentration phase, a Schumasiv type 5 nm pore size membrane for nanofiltration of the ultrafiltration retentate, and a Membralox type 5 kDa membrane for nanofiltration of the ultrafiltration permeate. The experiments were carried out using ultra- and nanofiltration units in a laboratory unit designed by the Department of Food Engineering. The effective area of the membranes was 0.005 m^2. The milk sample was circulated at a constant temperature (21±1 ºC) maintained by a thermostat. The optimal working parameters were measured during an experimental design in both the UF and NF processes. During the UF process the transmembrane pressure was 1.5 bars and the recirculation flow rate was 150 $dm^3\ h^{-1}$. In both NF processes, the transmembrane pressure was 2 bars and the recirculation flow rate was 200 $dm^3\ h^{-1}$. The transmembrane pressure and the recirculation flow rate were controlled by regulating valves.

2.2. Process simulation

The partial demineralization process was modelled using SuperPro Designer software version 8.5 by Intelligen, Inc. The main target task was partial demineralization. The SuperPro Designer software possesses an industrial tools section, where models of reactors, chemical components, a database of mixtures, price estimations and economic evaluations can be used.

Table 1. The characteristics of the membranes used.

Membrane type	Process parameters	
	Pressure, bar	Flow rate, $dm^3\ h^{-1}$
UF (100 nm)	1.5	150
NF (5 kDa)	2.0	200
NF (5 nm)	2.0	200

The parameters used were calculated from laboratory experiments as shown in *Table 1*.

Firstly, The SuperPro Designer tool was used to install the unit operations. The first unit is the ultrafiltration system. The raw milk enters the system and is separated into its permeate and retentate. In the next step, the two fractions are transferred to each diafiltration unit. Another major step is the definition of essential material streams for milk, the addition of distilled water to the diafiltration unit and the provision of electricity. The diafiltrated, partially demineralized milk and whey components are then sent to the storage tank. The last part of the process is the packaging system, where the products are completed. The demineralized whey is finally loaded into a truck. The mass of the filled entity is 40 metric tons (MT). The basic process flow diagram of the combined partial demineralization of cow milk is shown in *Fig. 1*. The composition of the milk was defined as illustrated in *Table 2*.

In the next step, the transmembrane pressure, flow rate and flux as operating parameters were set and the cost of purchase assigned to each operating unit. The annual operating time is 300 days for this process. The cost of purchase of the ultrafiltration system was set at $100k, the two diafiltration units at $75k, the storage

Table 2. The composition of the cow milk considered

Ingredient's name	Mass (%)
Casein	3.4
Fats	3.4
Lactose	5.2
Sodium Chloride	1.0
Water	87

Table 3. Cost estimates for energy supplies

Energy supplies	Price
Steam (High P) [242 ℃]	$10/MT
Steam [152 ℃]	$6/MT
Chilled Water [5 ℃ - 10 ℃]	$0.4/MT
Cooling Water [25 ℃ - 30 ℃]	$0.05/MT
Std. Power	$0.1/kWh

tanks at $75k, and the packaging unit at $50k. In addition, the cost of raw materials was set at $1/kg, of packaging material at $0.1/piece (100g), and of water at $0.1/kg. The product must be sold at a price that is in line with the market conditions (est. $2.2/kg). Each unit operation needs a minimum of one operator, thus the cost of labour was set at a basic rate of $10 per hour. The electricity, cooling and heating energy demands were estimated by the programme (*Table 3*).

3. Results and Analysis

Upon the establishment of costs, technological and economic simulations were executed. The summary of the run simulations for the partial demineralization process yielded the relevant costs, revenue and payback time as shown in *Table 4.* According to the simulation results, the annual total revenue is higher than the operating costs. The production costs are given with and without amortization. *Table 5* summarizes the indices of the project. The 'payback time' or 'return on investment' (ROI) for the partial demineralization process in this case was calculated for four years. The ROI is defined by *Eq. (1)*:

$$\text{ROI (\%)} = \frac{\text{annual net profit}}{\text{capital cost}} \cdot 100 \qquad (1)$$

Other important parameters were the 'internal rate of return' (IRR) before and after tax. The IRR is a discount value when the 'net present value' (NPV) is zero. The NPV is determined by calculating the costs and benefits of the technological investment. The NPV is defined by *Eq. (2)*:

$$\text{NPV (USD)} = \sum \frac{C_t}{(1+d)^t} - C_0 \qquad (2)$$

Table 4. Summary of economy indices (MP stands for "flow of discrete entity").

total investment	$6,279,438
total annual revenue	$30,315,042
annual operating cost	$28,258,168
annual unit production	$10,800,660
reference rate (MP entity)	
unit product cost (per MP entity)	
including depreciation	$2.62
excluding depreciation	$2.59

Table 5. Summary of project indices (IRR = internal rate of return, NPV = net present value).

gross margin, %	6.78
return on investment, %	24.90
payback time, years	4.02
IRR before tax, %	28.36
IRR after tax, %	18.20
NPV (at 7.00%)	5,381,025

where C_t is the cash flow, t is the lifetime in years, d is the discount rate, and C_0 is the initial investment. If the NPV remains positive, the process will be economically viable [8].

The costs of materials and supplies are shown in *Table 6* with the most expensive item being the raw material (cow milk) while the cost of packaging materials is far less. *Table 7* presents the total cost of the plant for the demineralization process. In addition to purchasing the equipment, other costs were the piping, instrumentation, and electrical, building and construction fees.

According to the simulated revenues of the partial demineralization process, the production of milk and lactose solution cost $2.2 and $0.3 per kg, respectively. Assuming that the demineralized whey is transferred into a truck, it can be sold to food industries for $40 per metric ton. The composition of the demineralised whey in the form of lactose solution is 4.3% lactose, 0.8% NaCl and 95% water, which is suitable for the production of candy, yoghurt and ice cream. It is also important to consider the cost of waste treatment. The SuperPro Designer generated two different costs, namely those of utilities ($25k) and transportation ($874k).

4. Conclusion

This study examined the feasibility of the partial demineralization process which was successfully

Table 6. Summary of the costs of materials (in USD per kg annually).

raw materials	unit	amount	cost
milk	$1.00	21,766,316	21,766,316
water	$0.10	10,879,641	1,087,964
packaging material	$0.20	10,800,661	2,160,132
total	-	-	25,014,412

Table 7. Total cost of the plant (in thousands of USD).

equipment purchase	$563k
installation	$266k
process piping	$197k
instrumentation	$225k
insulation	$17k
electrical	$56k
buildings	$253k
yard improvements	$84k
auxiliary facilities	$225k
engineering	$472k
construction	$66k

modelled by the SuperPro Designer software. According to an economic evaluation, the net present value, return on investment, and internal rate of return were \$5.3Million for four years, 28% and 18%, respectively. The revenues of the products were \$2.2 per unit and \$0.3 per kg (or \$40 per metric ton) for the milk and lactose solution, respectively. Future research will focus on the optimization of costs and exploration of alternative ways of recycling whey.

Acknowledgement

The research was supported by the Doctoral School of Food Sciences at Szent István University.

REFERENCES

[1] Csapo, J.; Csapone, K.Zs.: Milk and Dairy Products in Food Consumption (Mezőgazdasági Kiadó, Budapest) 2002 (in Hungarian) ISBN 963 9358 68 1

[2] Mass, S.; Lucot, E.; Gimbert, F.; Crini, N.; Badot, P.M.: Trace metals in raw cow's milk and assessment of transfer to Comté cheese, *Food Chem.*, 2011 **129**(1), 7–12 DOI: 10. 1016/j.foodchem.2010.09.034

[3] Suárez, E.; Lobo, A.; Álvarez, S.; Riera, F.A.; Álvarez, R.: Partial demineralization of whey and milk ultrafiltration permeate by nanofiltration at pilot-plant scale, *Desalination*, 2006 **198**(1-3), 274–281 DOI 10.1016/j.desal.2005.12.028

[4] Tsakali, E.; Petrotos, K.; Alessandro, A.D.; Goulas, P.: A review on whey composition and methods used for its utilization for food and pharmaceutical products, *Proc. 6th Int. Conf. Simul. Modelling Food Bioind.,* 2010 (CIMO Research Centre, Bragança, Portugal) pp. 195-201

[5] Pan, K.; Song, Q.; Wang, L.; Cao, B.: A study of demineralization of whey by nanofiltration membrane, *Desalination*, 2011 **267**(2-3), 217–221 DOI 10.1016/j.desal.2010.09.029

[6] Mel, M.; Yong, A.S.H.; Avicenna; Ihsan, S.I.; Setyobudi, R.H.: Simulation Study for Economic Analysis of Biogas Production from Agricultural Biomass, *Energy Procedia*, 2015 **65**, 204-214 DOI 10.1016/j.egypro.2015.01.026

[7] Flora, J.R.V.; McAnally, S.A.; Petrides, D.: Treatment plant instructional modules based on SuperPro Designer® v.2.7, *Environ. Model. Software*, 1998 **14**(1), 69–80 DOI 10.1016/S1364-8152(98)00059-0

[8] Kwan, T.H.; Pleissner, D.; Lau, K.Y.; Venus, J.; Pommeret, A.; Lin, C.S.: Techno-economic analysis of a food waste valorization process via microalgae cultivation and co-production of plasticizer, lactic acid and animal feed from algal biomass and food waste, *Biores. Technol.*, 2015 **198**, 292–299 DOI 10.1016/j.biortech.2015.09.003

DE GRUYTER

HUNGARIAN JOURNAL OF INDUSTRY AND CHEMISTRY
Vol. 45(2) pp. 13–18 (2017)
hjic.mk.uni-pannon.hu
DOI: 10.1515/hjic-2017-0014

HUNGARIAN JOURNAL OF INDUSTRY AND CHEMISTRY
HJIC

INVESTIGATIONS OF THE $TlInP_2Se_6$–$In_4(P_2Se_6)_3$ SYSTEM AND ITS OPTICAL PROPERTIES

VALERIA TOVT,[1] IGOR BARCHIY,[1]* MICHAL PIASECKI,[2] IWAN KITYK,[3] AND ANATOLII FEDORCHUK[4]

[1] Department of Chemistry, Uzhgorod National University, Pidgirna St. 46, 88000 Uzhgorod, UKRAINE
[2] Institute of Physics, Jan Dlugosz University, Armii Krajowej 13/15, 42-200 Częstochowa, POLAND
[3] Faculty of Electrical Engineering, Częstochowa University of Technology, Dabrowskiego 69, 42201 Częstochowa, POLAND
[4] Department of Inorganic and Organic Chemistry, Lviv National University of Veterinary Medicine and Biotechnologies, Pekarska St. 50, 79010 Lviv, UKRAINE

The equilibrium phases were investigated and the corresponding phase diagram constructed for the $TlInP_2Se_6$–$In_4(P_2Se_6)_3$ system from physical and chemical analyses, namely differential thermal analysis (DTA), X-ray diffraction (XRD), and microstructural analysis (MSA). It was established that this system belongs to the eutectic type and is characterized by the formation of boundary solid phases containing complex compounds. Single crystals of the compounds $TlInP_2Se_6$ and $In_4(P_2Se_6)_3$ were grown using the Bridgman method. Both crystals were found to exhibit diffuse reflection spectra and photoinduced dependence of birefringence at various IR wavelengths generated by CO_2 laser irradiation. Birefringence properties were investigated using the Senarmont method.

Keywords: phase diagram, solid solution, crystal structure, optical properties, direct-gap semiconductor, indirect-gap semiconductor, photoinduced birefringence

1. Introduction

Compounds with the formula $M_2P_2Se_6$ possess promising magneto-electric, piezoelectric, electro-optical, and thermoelectric properties that indicate their suitability as functional materials in optoelectronics [1-2]. Due to their crystal structure, they exhibit anisotropy in terms of their physical properties. In a multilevel structure of $M_2P_2Se_6$ compounds, metal cations and pairs of phosphorous atoms occupy the octahedral positions between planes of selenium atoms. This structure is characterized by its layered arrangement of atoms, which contributes to the formation of a dipole moment between the layers of cationic and anionic groups. The replacement of the metal cation M^{2+} by other metal cations (M^{+}, M^{3+} or M^{4+}) leads to the deformation of the structure [3-4], changes the magnitude of the dipole moment and, consequently, its physical properties.

The Tl_2Se–In_2Se_3–"P_2Se_4" ternary system is composed of binary Tl_2Se–In_2Se_3, Tl_2Se–"P_2Se_4" and In_2Se_3–"P_2Se_4" systems. The Tl_2Se–In_2Se_3 system is characterized by the formation of two intermediate ternary compounds: $TlInSe_2$ melts congruently at 1023 K and $TlIn_5Se_8$ is formed according to the peritectic reaction L + In_2Se_3 ↔ $TlIn_5Se_8$ at 1029 K [5-6]. In the system Tl_2Se–"P_2Se_4" with a ratio of 2 to 1, interoperable components form the compound $Tl_4P_2Se_6$ which possesses a congruent nature of melting at 758 K [7]. The In_2Se_3–"P_2Se_4" system is characterized by the formation of the compound $In_4(P_2Se_6)_3$ in a syntectic reaction of L1 + L2 ↔ $In_4(P_2Se_6)_3$ at 880 K [8]. In the Tl_2Se–In_2Se_3–"P_2Se_4" system at the intersection of incisions, the phases $Tl_4P_2Se_6$–$In_4(P_2Se_6)_3$ and $TlInSe_2$–"P_2Se_4" form the complex compound $TlInP_2Se_6$ [9].

*Correspondence: i_barchiy@ukr.net

2. Experimental

Ternary $Tl_4P_2Se_6$ and $In_4(P_2Se_6)_3$ compounds were prepared by melting stoichiometric quantities of binary Tl_2Se with elementary indium, phosphorous and selenium under a vacuum of 0.13 Pa in quartz ampoules using a single temperature method. In all syntheses, components were used that possess a purity greater than 99.999 %. The maximum temperatures of synthesis were 993 and 893 K for $In_4(P_2Se_6)_3$ and $TlInP_2Se_6$, respectively. The rate of heating up to the maximum temperature was 50 K h^{-1}. The melts were maintained at the maximum temperature for 72 hours. Cooling was performed at a rate of 50 K h^{-1} down to an annealing temperature of 573 K. The linearity of the heating and cooling processes was achieved by a RIF-101 temperature controller. The homogenization process occurred over 120 hours. Identification of the complex compounds and alloys was conducted by differential thermal analy-

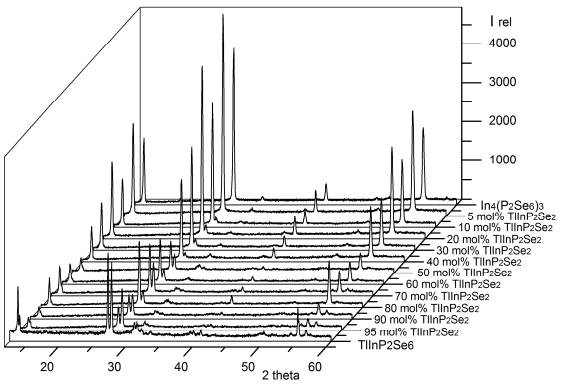

Figure 1. Results of the XRD analysis of the $TlInP_2Se_6$–$In_4(P_2Se_6)_3$ system. (I rel – Intensity, 2 theta - Angle of reflection)

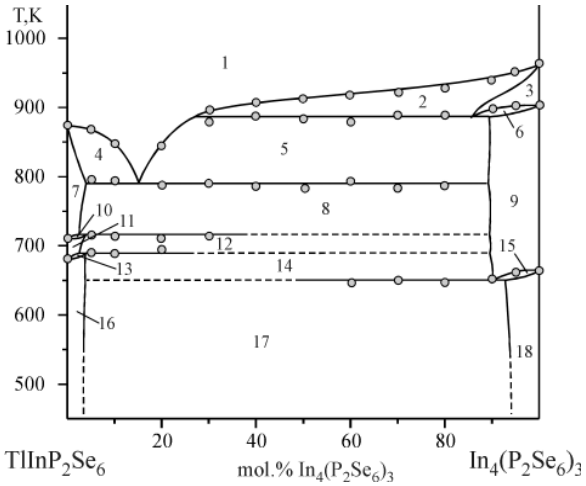

Figure 2. Phase diagram of the $TlInP_2Se_6$–$In_4(P_2Se_6)_3$ system. (1–L, 2–L+*ht*$In_4(P_2Se_6)_3$, 3–*ht*$In_4(P_2Se_6)_3$, 4–*ht*$TlInP_2Se_6$, 5–L+*mt*$In_4(P_2Se_6)_3$, 6–*ht*$In_4(P_2Se_6)_3$+*mt*$In_4(P_2Se_6)_3$, 7–*ht*$TlInP_2Se_6$, 8–*ht*$TlInP_2Se_6$+*mt*$In_4(P_2Se_6)_3$, 9–*mt*$In_4(P_2Se_6)_3$, 10–*ht*$TlInP_2Se_6$+*mt*$TlInP_2Se_6$, 11–*mt*$TlInP_2Se_6$, 12–*mt*$TlInP_2Se_6$+*mt*$In_4(P_2Se_6)_3$, 13–*mt*$TlInP_2Se_6$+*lt*$TlInP_2Se_6$, 14–*lt*$TlInP_2Se_6$+*mt*$In_4(P_2Se_6)_3$, 15–*mt*$In_4(P_2Se_6)_3$+lt$In_4(P_2Se_6)_3$, 16–*lt*$TlInP_2Se_6$, 17–*lt*$TlInP_2Se_6$+*lt*$In_4(P_2Se_6)_3$, 18–*lt*$In_4(P_2Se_6)_3$).

sis (DTA) (PRA-01, chrome-alumina thermocouple ±5 K), X-ray diffraction (XRD) (DRON-3 diffractometer, CuKα radiation, Ni filter) and microstructural analysis (MSA) (metallurgical microscope Lomo Metam R-1). Crystal structural calculations were conducted using the software package WinCSD [10]. Optical properties were investigated using an SF-18 spectrophotometer within the wavelength range of 400 – 750 nm. A CO_2 laser was used for photoinduced electrons in samples employing 200 ns pulses with a pulse repetition frequency of about 10 Hz, a fundamental frequency of 10.6 μm and a frequency doubling of 5.3 μm beams. The birefringence was measured using a Er:glass cw laser at 1540 nm by application of the Senarmont method.

3. Results and Analysis

3.1. Phase diagram of the $TlInP_2Se_6$–$In_4(P_2Se_6)_3$ system

The $TlInP_2Se_6$–$In_4(P_2Se_6)_3$ system is a quasi-binary section of the Tl_2Se–In_2Se_3–"P_2Se_4" ternary system (*Figs.1* and *2*). It belongs to the eutectic type (V-type diagram by Rozeboom). The complex compounds $TlInP_2Se_6$ and $In_4(P_2Se_6)_3$ melt congruently at 875 K and 963 K, respectively. $TlInP_2Se_6$ is characterized by two polymorphic transformations *lt*$TlInP_2Se_6$ ↔ *mt*$TlInP_2Se_6$ at 680 K and *mt*$TlInP_2Se_6$ ↔ *ht*$TlInP_2Se_6$ at 711 K. The prefixes *lt–, mt–* and *ht–* represent low–, medium–, and high–temperature modifications, respectively. $In_4(P_2Se_6)_3$ is also characterized by two polymorphic transformations *lt*$In_4(P_2Se_6)_3$ ↔ *mt*$In_4(P_2Se_6)_3$ at 665 K and *mt*$In_4(P_2Se_6)_3$ ↔ *ht*$In_4(P_2Se_6)_3$ at 903 K. When the temperature rises above 791 K, an invariant eutectic process is observed L ↔ *ht*$TlInP_2Se_6$ + *mt*$In_4(P_2Se_6)_3$ (in the presence of 15 mol% $In_4(P_2Se_6)_3$).

The system is described by the sequence of the efficient peritectic processes *ht*$TlInP_2Se_6$ + *mt*$In_4(P_2Se_6)_3$ ↔ *mt*$TlInP_2Se_6$ (714 K) and *mt*$TlInP_2Se_6$ + *mt*$In_4(P_2Se_6)_3$ ↔ *lt*$TlInP_2Se_6$ (689 K) based on the polymorphic transformation of $TlInP_2Se_6$. The polymorphism of $In_4(P_2Se_6)_3$ produces metatectic *ht*$In_4(P_2Se_6)_3$ ↔ L + *mt*$In_4(P_2Se_6)_3$ (884 K) and eutectic *mt*$In_4(P_2Se_6)_3$ ↔ *lt*$TlInP_2Se_6$ + *lt*$In_4(P_2Se_6)_3$ (652 K) processes. Regions of homogeneity in solid solutions, based on the batched complex selenides during annealing at a temperature of 573 K, do not exceed 10 mol%.

3.2. Crystal structure of the compounds $In_4(P_2Se_6)_3$ and $TlInP_2Se_6$

The crystal structures of the compounds $TlInP_2Se_6$ and $In_4(P_2Se_6)_3$ were solved using the Rietveld method. As an initial model for $TlInP_2Se_6$ [2], the parameters of $In_4(P_2Se_6)_3$ were used [8]. Analysis of the crystalline structures of the investigated compounds (*Table 1*) showed that it is possible to define the structural group of the anionic group $[P_2Se_6]^{4-}$, which is formed by two single tetrahedra (*Fig.3*). Cationic atoms occupy positions between the anionic groups and none are located between the layers.

Table 1. Crystal data of $TlInP_2Se_6$ and $In_4(P_2Se_6)_3$ compounds.

Compound	Crystal system	Space group	Lattice constant
$In_4(P_2Se_6)_3$ [8]	trigonal	*R*3 h (146)	a = 6.362(3), c = 19.929(6) Å
$In_4(P_2Se_6)_3$	trigonal	*R*3 h (146)	a = 6.3808(8), c = 20.014(4) Å
$TlInP_2Se_6$ [2]	triclinic	*P*-1 (2)	a = 6.4310, b = 7.5002, c = 12.124 Å,
$TlInP_2Se_6$	triclinic	*P*-1 (2)	α = 100.553, β = 93.735, γ = 113.451

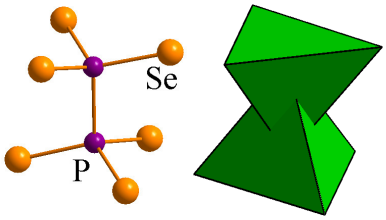

Figure 3. Structure of the anionic group $[P_2Se_6]^{4-}$.

The structure of $In_4(P_2Se_6)_3$ can be derived from the structure of $Sn_2P_2Se_6$ [11]. It is composed of multiple substitutions of the isovalent cations according to $2M^{2+} \leftrightarrow M^{4+}$. The crystal structure of the compound $In_4(P_2Se_6)_3$ can be presented based on the composition of the anionic group $[P_2Se_6]^{4-}$ (*Fig.4*), in which the indium atoms occupy the space between the anionic groups.

The second coordination environment (SCE) [12] is of cuboctahedron form. Indium cations are surrounded by a triangular environment of anionic atoms of the group $[P_2Se_6]^{4-}$and within the frames of its environment bonding exists with six atoms of selenium while the coordination form is octahedral (*Fig.5*).

The structural and chemical properties of the $Me^{I}Me^{III}P_2Se_6$ compositions are related to the important role concerning the dimension of the cation on its location between the layers of the anionic $[P_2Se_6]^{4-}$groups. Crystallographic analysis showed that smaller cations occupy a position in the plane perpendicular to the main axis. Atoms located in a second coordination environment of anionic groups in the structure of $TlInP_2Se_6$ compounds can be presented as a strongly distorted hexagonal-equivalent cuboctahedron (*Fig.6*).

The atoms of metallic cations, located in the cavities between the atoms of the anionic groups, are within an asymmetric environment (*Fig.7*). In^{3+} cations move toward tetrahedral cavities on the boundary between

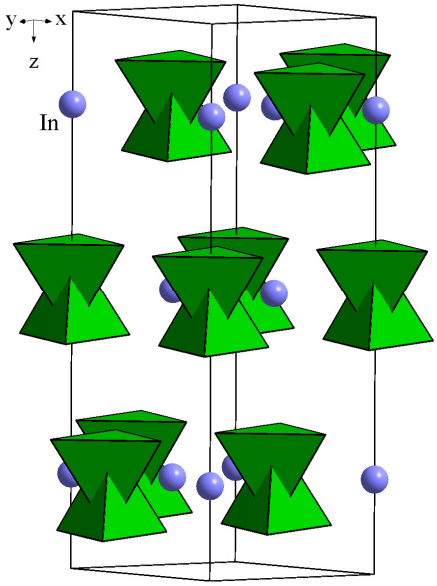

Figure 4. Arrangement of the polyhedra anionic group $[P_2Se_6]^{4-}$ in $In_4(P_2Se_6)_3$.

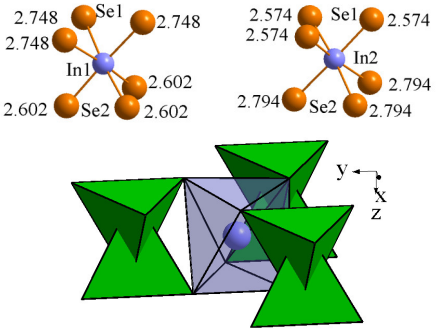

Figure 5. Coordination environment of the indium atoms in the structure of $In_4(P_2Se_6)_3$.

tetrahedral and octahedral cavities, and Tl^{+} cations move in the direction of the octahedral cavities.

Moreover the In^{3+} cations are located in the same plane together with the centres of the anionic $[P_2Se_6]^{4-}$ groups (*Fig.8*) and some Tl^{+} cations are shifted relative to the plane. Therefore, this arrangement is a source of the interesting electro-physical and optical properties of materials based on compounds of this type.

3.3. Optical response of single crystals of $TlInP_2Se_6$ and $In_4(P_2Se_6)_3$

The most important parameter of the energy spectra of semiconductors is the width of the band gap, E_g, which is defined by the difference in energy between the bottom of the conduction band, E_C, and the top of the valence band, E_V. All semiconductors can be divided into two groups. In the first group, the minimum of the conduction band and the maximum of the valence band occupy the same point in the Brillouin zone, i.e. at an identical location in the space of quasi-moments. In this case, the optical transitions of electrons from the valence band to the conduction band (with the absorption of a quantum of light) and from the conduction band to the valence band (with the emission of a quantum of light) occur so that the electrons practically do not change their quasi-moments. Such transitions are characteristic of direct-gap semiconductors. For the second group, the absolute minimum of the conduction band and the absolute maximum of the valence band are at different points in the Brillouin zone, and optical inter-

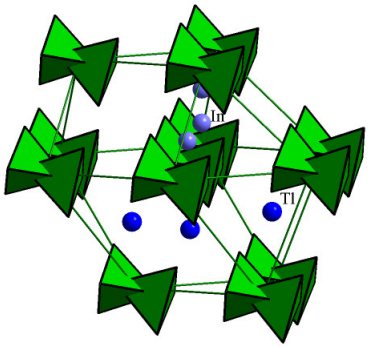

Figure 6. Second (SCE) and nearest (NCE) coordination environments of atoms in the $[P_2Se_6]^{4-}$ anionic groups in the structure of $TlInP_2Se_6$.

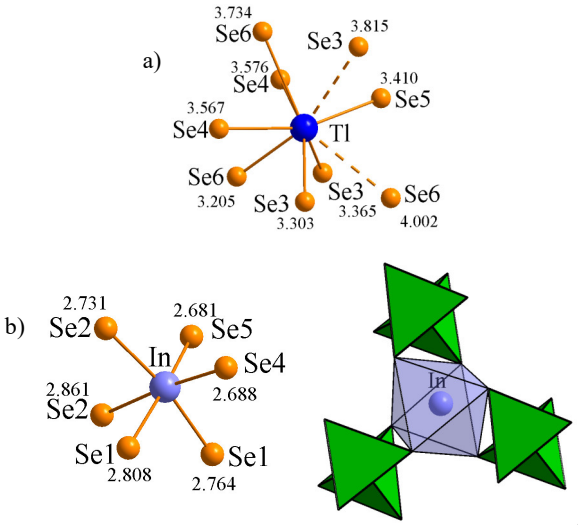

Figure 7. Coordination environments of the thallium (a) and indium (b) atoms in the structure of $TlInP_2Se_6$.

band transitions must be accompanied by a large change in the electron quasi-moment. These are characteristic of indirect-gap semiconductors. Since the photon moment is negligibly small compared with the electron quasi-moment, the latter case is possible only when the electron interacts with the phonon.

According to the phase diagram, the single crystals of $TlInP_2Se_6$ and $In_4(P_2Se_6)_3$ were grown using the Bridgman method in two vertical zone furnaces. Experimental studies of optical spectra in the absorption region yielded information on the energy spectrum of electrons near the edges of the conduction band and band gap. Studies concerning the dependence of diffuse reflection on wavelength ($R = f(\lambda)$) have shown that the compound $TlInP_2Se_6$ refers to indirect-gap semiconductors. On the graph there are two rectilinear sections, one of which (for small wavelengths, λ, and large values of E) characterizes the interband transitions of electrons with phonon emission, and the other (for large λ and small E) describes the processes of phonon absorption (*Fig.9*).

The intersection of the first section with the wavelength axis, λ, yields the value of $E_g + E_{phonon}$ (λ = 560 nm, E = 2.21 eV), and the intersection of the second

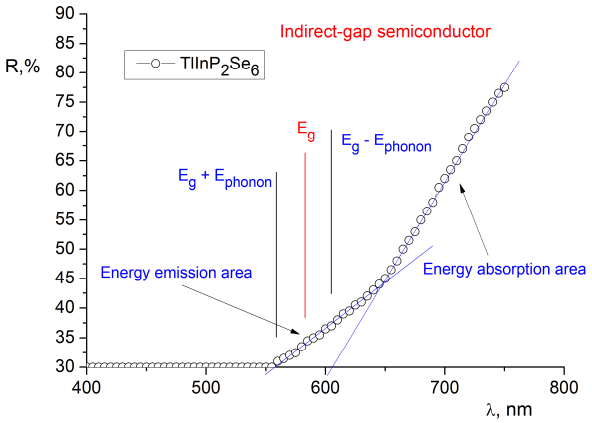

Figure 9. Dependence of the diffuse reflection R on the wavelength λ for the compound $TlInP_2Se_6$.

characterizes $E_g - E_{phonon}$ (λ = 605 nm and E = 2.05 eV). The length of the segment between the points of intersection of both straight lines with the wavelength axis, λ, is equal to the doubled energy of the phonons, $2E_{phonon}$ (0.16 eV), interacting with the electron. The middle of this segment corresponds to the photon energy equal to the width of the band gap of the indirect-gap semiconductor, E_g. Experimental calculations in terms of the compound $TlInP_2Se_6$ have shown that E_g = 2.13 eV and E_{phonon} = 0.08 eV.

The compound $In_4(P_2Se_6)_3$ refers to direct-gap semiconductors, which characterizes the interband transitions of electrons in terms of photon absorption (*Fig.10*). The intersection of the line with the wavelength axis, λ (λ = 651 nm), yields the value of E_g = 1.91 eV.

The crystals of $In_4(P_2Se_6)_3$ and $TlInP_2Se_6$ were illuminated by 10.6 μm and (its second harmonic) frequency doubling of 5.3 μm beams. Each channel of the beam was split by 200-ns CO_2 laser pulses with a pulse repetition frequency of about 10 Hz. The angle between these two laser beams was changed from 18° to 22°. *Figs.11* and *12* present these dependences. Treatment with a 10.6 μm beam achieved a smaller maximum birefringence (about 1.55×10^{-2}) in comparison to the 5.2 μm beam. This indicates a different photoinduced anisotropy for the $In_4(P_2Se_6)_3$ and $TlInP_2Se_6$ crystals. Because

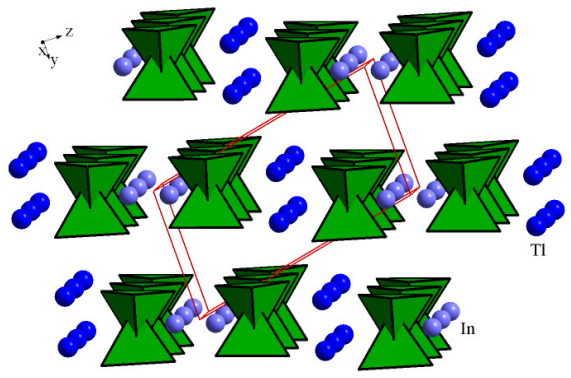

Figure 8. Arrangement of the polyhedra anionic group $[P_2Se_6]^{4-}$ in the structure of $TlInP_2Se_6$.

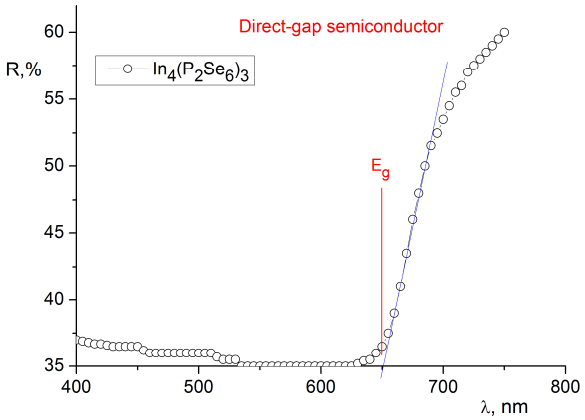

Figure 10. Dependence of the diffuse reflection R on the wavelength λ for the compound $In_4(P_2Se_6)_3$.

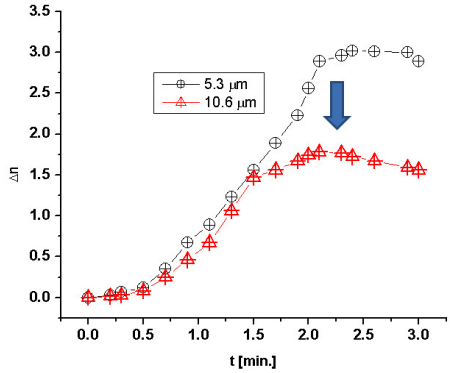

Figure 11. Photoinduced birefringence dependence at wavelengths of 5.3 μm and 10.6 μm - the two coherent beams were illuminated under different angles. During the two-beam coherent treatment at optimal power densities (about 400 MW/cm^2) and incident angles (18-22 degrees) for crystals of $In_4(P_2Se_6)_3$. The birefringence scale should be multiplied by 10^{-2}.

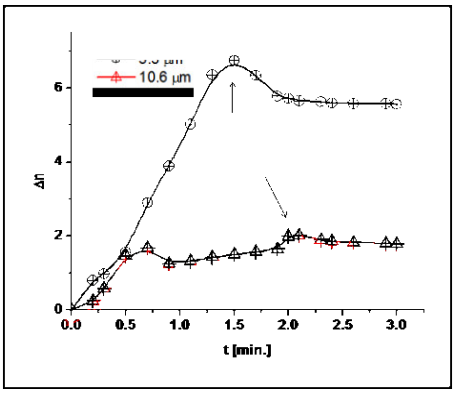

Figure 12. Photoinduced birefringence dependence at wavelengths of 5.3 μm and 10.6 μm - the two coherent beams were illuminated under different angles. During the two-beam coherent treatment at optimal power densities (about 400 MW/cm^2) and incident angles (18-22 degrees) for crystals of $TlInP_2Se_6$. The birefringence scale should be multiplied by 10^{-2}.

these crystals contain chalcogenide anions that contribute to the anharmonicity of the phonon, they play a crucial role in terms of the second harmonic generation [13-14]. The maximum changes in the birefringence achieved were less than 2×10^{-2} and 6.3×10^{-2} for CO_2 laser wavelengths of 10.6 μm and 5.3 μm, respectively.

4. Conclusion

Differential thermal analysis, X-ray diffraction and microstructural analysis were used to construct a phase diagram for the $TlInP_2Se_6$–$In_4(P_2Se_6)_3$ system, which can be characterized by a eutectic-type interaction. The invariant eutectic process L ↔ *ht*$TlInP_2Se_6$ + *mt*$In_4(P_2Se_6)_3$ (15 mol% $In_4(P_2Se_6)_3$) occurs at 791 K. Two polymorphic transformations were identified for $TlInP_2Se_6$ at 680 K and 711 K and for $In_4(P_2Se_6)_3$ at 665 K and 903 K. New compounds were not detected in the binary system. The regions of solid phases of the complex compounds $TlInP_2Se_6$ and $In_4(P_2Se_6)_3$ do not exceed 10 mol%. Single crystals of both test compounds were achieved by the Bridgman method. Investigations concerning the dependence of the diffuse reflection spectrum showed that the compound $TlInP_2Se_6$ is characteristic of indirect-gap semiconductors (E_g = 2.13 eV, E_{phonon} = 0.08 eV), while the compound $In_4(P_2Se_6)_3$ is characteristic of direct-gap semiconductors (E_g = 1.91 eV, E_{phonon} = 0.08 eV). The dependence of the birefringence was photoinduced by wavelengths of 5.3 μm and 10.6 μm, which is indicative of different photoinduced anisotropy.

Acknowledgement

We are grateful for the financial support of this work by the Ministry of Education and Science of Ukraine under the project DB874P_0117U000380.

SYMBOLS

ht	high–temperature modification
mt	middle–temperature modification
lt	low–temperature modification
SCE	second coordination environment
NCE	nearest coordination environment
E_g	band gap, eV
E_{phonon}	phonon energy, eV
R	diffuse reflection
λ	wavelength, nm

REFERENCES

[1] Galdamez, A., Manriquez, V., Kasaneva, J., Avila, R.E.: Synthesis, characterization and electrical properties of quaternary selenodiphosphates: AMP2Se6 with A – Cu, Ag and M – Bi, Sb, *Mat. Res. Bull.*, 2003 **38**, 1063-1072 DOI: 10.1016/S0025-5408(03)00068-0

[2] McGuire, M.A.; Reynolds, T.K.; Di Salvo, F.J.: Exploring thallium compounds as thermoelectric materials: seventeen new thallium chalcogenides, *Chem. Mater.*, 2005 **17**, 2875-2884 DOI: 10.1021/cm050412c

[3] Gave, M.A.; Bilc, D.; Mahanti, S.D.; Breshears, J.D.; Kanatzidis, M.G.: On the lamellar compounds $CuBiP_2Se_6$, $AgBiP_2Se_6$ and $AgBiP_2S_6$. antiferroelectric phase transitions due to cooperative Cu^+ and Bi^{3+} ion motion, *Inorg. Chem.*, 2005 **44**, 5293-5303 DOI: 10.1021/ic050357

[4] Pfeiff, R.; Kniep, R.: Quaternary selenodiphosphates(IV): M(I)M(III)[P_2Se_6], (M(I) = Cu, Ag; M(III) = Cr, Al, Ga, In), *J. Alloys Compd.*, 1992 **186**, 111-133 DOI: 10.1016/0925-8388(92)90626-K

[5] Mucha, I.: Phase diagram for the quasi-binary thallium(I) selenide–indium(III) selenide system, *Thermochimica Acta*, 2012 **550**, 1-4 DOI: 10.1016/j.tca.2012.09.028

[6] Guseinov, G.D.; Abdullaev, G.B.; Godzhaev, E.M.; Rzaeva, L.A.; Agaev, G.A.: Constitutional diagram and physical properties of thallium selenide–indium selenide pseudobinary system, *Mater. Res. Bull.*, 1972 **7(12)**, 1497-1503 DOI: 10.1016/0025-5408(72)90187-0

[7] Brockner, W.; Ohse, L.; Pätzmann, U.; Eisenmann, B.; Schäfer, H.: Kristallstruktur und Schwingungsspektrum des Tetra-Thallium-Hexaselenidohypodiphosphates $Tl_4P_2Se_6$, *Z. Naturforsch. A*, 1985 **40**, 1248-1252

[8] Voroshilov, Y.V.; Gebesh, V.Y.; Potorii, M.V.: Phase equilibria in the system In–P–Se and crystal structure of β-$In_4(P_2Se_6)_3$, *Inorg. Mater.*, 1991 **27**, 2141-2144

[9] Tovt, V.A.; Barchiy, I.E.; Piasecki, M.; Kityk, I.V.; Fedorchuk, A.O.; Solomon, A.M.; Pogodin, A.I.: Triangulation of the Tl_2Se–In_2Se_3–"P_2Se_4" quasiternary system, *Nauch. Vestn. Uzhgorod. Univ. (Ser. Khim.)*, 2016 **35(2)**, 14–19 (in Russian)

[10] Akselrud, L.; Grin, Y.: WinCSD: Software package for crystallographic calculations (Ver.4), *J. Appl. Crystallogr.*, 2014 **47**, 803-805 DOI: 10.1107/S1600576714001058

[11] Israel, R.; De Gelder, R.; Smits, J.M.M.; Beurskens, P.T.; Eijt, S.W.H.; Rasing, T.H.; van Kempen, H.; Maior, M.M.; Motrya, S.F.: Crystal structures of di-tin-hexa(seleno)hypodiphosphate, $Sn_2P_2Se_6$, in the ferroelectric and paraelectric phase, *Z. Kristallogr.*, 1998 **213**, 34-41 DOI: 10.1524/zkri.1998.213.1.34

[12] Fedorchuk, A.O.; Parasyuk, O.V.; Kityk, I.V.: Second anion coordination for wurtzite and sphalerite chalcogenide derivatives as a tool for the description of anion sub-lattice, *Mat. Chem. Phys.*, 2013 **139**, 92-99 DOI: 10.1016/j.matchemphys.2012.12.058

[13] Kityk, I.V.: IR-stimulated second harmonic generation in Sb_2Te_2Se–BaF_2–$PbCl_2$ glasses, *J. Modern Optics,* 2004 **51**, 1179-1189 DOI: 10.1080/09500340408230415

[14] Kityk, I.V.: IR-induced second harmonic generation in Sb_2Te_3–BaF_2–$PbCl_2$ glasses, *J. Phys. Chem. B*, 2003 **107**, 10083-10087 DOI: 10.1021/jp030058a

DE GRUYTER

HUNGARIAN JOURNAL OF INDUSTRY AND CHEMISTRY
Vol. 45(2) pp. 19–21 (2017)
hjic.mk.uni-pannon.hu
DOI: 10.1515/hjic-2017-0015

HUNGARIAN JOURNAL OF INDUSTRY AND CHEMISTRY
HJIC

EXAMINATION OF INNOVATIVE HIGH-THROUGHPUT FERMENTATIONS

ÁRON NÉMETH*

Department of Applied Biotechnology and Food Science, Budapest University of Technology and Economics, Műegyetem rkp. 3, Budapest, 1111, HUNGARY

During the investigation of fermentations, issues such as the need for numerous parallel experiments with regard to strain improvement or screening were often met, or in the case of media optimization the need for online measurements to avoid a lack of night-samples was also required. Therefore, several new instruments were introduced to solve one or more of these problems: impedimetric- and reverse-spin-technologies (RST) were compared *via* fermentation of a well-known species of yeast, *Saccharomyces cerevisiae,* under both aerobic and anaerobic conditions, resulting in a diauxic growth curve. To identify the most accurate method, a well-known mathematical description was fitted to the measured data. Since the initial parameters were considered reliable as they originated from real experiments, during model fitting, the parameters were further fine-tuned, and the less modifications reported the better the system since it produces a growth curve that is more similar to standard bioreactors. According to our study, the impedimetric equipment was more efficient, and could run 40 parallel experiments, but the RST was more flexible.

Keywords: fermentation, high-throughput, scale-down, online measurement, mathematical modelling

1. Introduction

Developments in fermentations face numerous challenges which may require expensive analytics, media components or special tools to facilitate aseptic work and sampling. Furthermore, these biological processes vary significantly. To overcome these difficulties, the process should be scaled-down in combination with high-throughput methods, resulting in many parallel, small-scale experiments. Such experiments are used in terms of strain and technological improvements as well as media optimization.

A good solution may be the consideration of micro-bioreactors. However, because of their high investment and operational costs, they have not become widespread in Hungary. While each can provide almost every service required for bioreactors, for example, aeration, agitation and sampling in addition to pH and temperature control, they possess considerable limitations, namely non-standard conformations resulting in scale-up difficulties, or special measurement techniques that are incompatible with standard methods.

A readily available alternative, to be more precise, Microtiter-Plates (MTP), for microscale high-throughput fermentations has already been presented and reported [1]. The basic principle is to use sterile ’96-Well’ microtiter plates with a special “sandwich cover” that facilitate sufficient aeration but reduce the likelihood of cross-infection. This system requires an adapter to be able to mount microtiter plates into a commercial rotary incubator shaker. The next issue is to analyse and follow the processes in the wells since their volumes are so small (*ca.* 100 μL) that sampling is impossible. Therefore, either a microplate reader is required or a simple office scanner to produce a grey-scale photo taken from the bottom of the plate. The colour of high cell-densities is close to white, but empty broths have a black background. In the case of species that produce high levels of acid, like *Lactobac*illus, even a pH indicator can be applied and besides a grey-scale photo a coloured one has to be taken as well; alternatively, $CaCO_3$ should be added at the start but this can disturb the scanner-based “photometry”.

Our partner (enzyscreen.com) even offers microtiter plates for fed-batch fermentations. To achieve this, the feed components are adsorbed onto the material of the MTP, and are programmed to slowly release the fresh substrate during cultivation. However, another innovative solution has been developed for small-scale fermentations using online monitoring: Biosan Ltd. (Lithuania) applies Reverse-Spin Technology in the equipment of their Personal Bioreactor (RTS-1). This cost-effective equipment rotates a standard Falcon tube, filled with *ca.* 10 ml of fermentation media, at different rotation speeds in several directions at various controlled temperatures using a variety of aeration holes on the cap. This instrument also involves a photometer to facilitate the programming of measuring frequencies at a given wavelength (λ = 850 nm). For calibrated and reproducible measurements, a constant film layer is necessary, therefore, the instruments increase the rate of

*Correspondence: naron@f-labor.mkt.bme.hu

rotation until 2000 rpm. The changes in parameters effect shear forces as well as levels of aeration.

Finally, this comparative study used an impedimetric system by SY-LAB (Austria) which is called BacTrac 4100 [2]. This equipment possesses a block thermostat composed of 40 measurement cells, each containing 4 electrodes. One pair of them follows the changes in the impedance of the media, M%, caused by the secreted acids and metabolites. In the case of microorganisms that exhibit high levels of ionic strength in the media, it is hard to detect M%, therefore, with the application of a different frequency the changes in impedance on the other electrode surface (E%) can be followed. In direct measurements, these electrodes are immersed directly into the culture, but in the case of indirect measurements, they are rinsed with KOH which can adsorb the formed CO_2 released by the culture. While this system does not possess mixer/aerator solutions, this result can be transferred carefully to the known systems, namely benchtop fermenters or shaking flasks. However, it is able to follow forty different cultures.

In this study, a well-known model organism (*S. cerevisiae*) was chosen that exhibits special biochemical behaviour. It was used to test the compare the ability of the three systems introduced above. What is special about *S. cerevisiae* is that it can change from aerobic to anaerobic cultivation according to Pasteur and Crabtree effects; i.e. under lack of oxygen or excess to sugar, respectively. After changing to anaerobic metabolism, it produces mostly alcohol but later this can be consumed by yeast as well resulting in a stepwise growth curve, also referred to as a diauxic growth profile. Thus, the question was whether such a system could show and follow this diauxic growth.

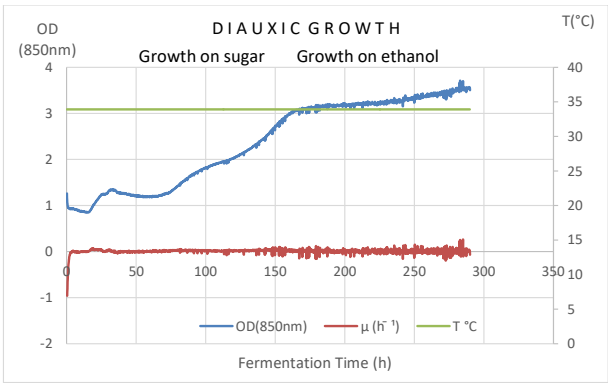

(A)

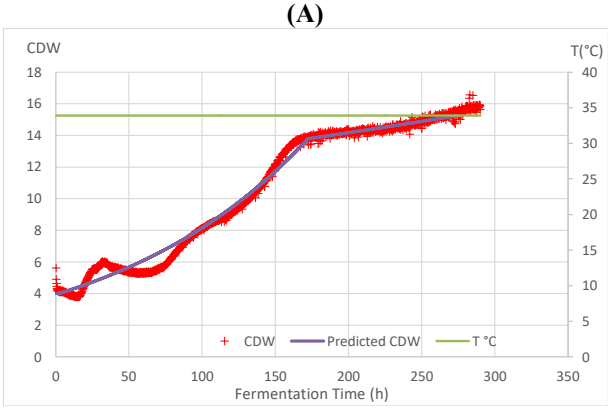

(B)

Figure 1. The measured parameters (temperature, μ, OD_{850}) and calculated data (CDW from OD_{850}) along with the data of the predicted (i.e. fitted) model. (A) green line: temperature; blue line: measured turbidity at 850nm; brown line: measured specific growth rate. (B) green line: temperature; red crosses: calculated cell dry weight from the measured turbidity at 850nm; purple line: fitted model-based prediction for CDW.

2. Experimental

Commercial *S. cerevisiae*, i.e. baking yeast produced by Lesaffre, was cultured on a media of molasses that were diluted by a factor of 10 resulting in a saccharose concentration of ca. 75 g dm^{-3} and a 20:1 volume of molasses to NH_4OH ratio at 34°C. The 100 μL of inoculum possessed a cell-dry-weight (CDW) content of 10 g/dm^3. RTS-1 collected the data in a Microsoft Excel database. BacTrac only provided the data collected on screen plots, but with the help of Digitizelt v.2.3 software the measurement data was transported into Microsoft Excel. To compare the data in Microsoft Excel, the structured model of Blanch et al. [3] was adopted and programmed in Berkeley Madonna for Windows 8.1. This model can describe both anaerobic cell growth on excess sugar with the formation of alcohol and aerobic cell growth on alcohol as a substrate. It divides cells into two main compartments, i.e. substructures: one is responsible for metabolism (both aerobic and anaerobic), and the other is responsible for cell division. The parameters, for example reciprocal yields and stoichiometric coefficients of the model, were partly determined experimentally, but others were determined by non-linear model fitting, i.e. model calibration on real samples.

3. Results and Analysis

3.1. Reverse-Spin Technology vs. Personal Bioreactor (RTS-1)

Fig.1 presents the results of RTS-1. While optical density (OD), i.e. turbidity at λ = 850nm, changed slowly, the specific growth rate calculated online only reflected the uncertainty of the OD measurements, but the temperature remained constant as expected. Additionally diauxic growth was also detected but over a very long period of time. The model fitting was quite difficult because a satisfactory fit was only achieved after remarkable changes to basic constants, for example maximum specific growth rates on both substrates, etc., had been applied.

3.2. Impedimetric System: BacTrac

In the case of the impedimetric experiments, three different arrangements were tested: an anaerobic cell with

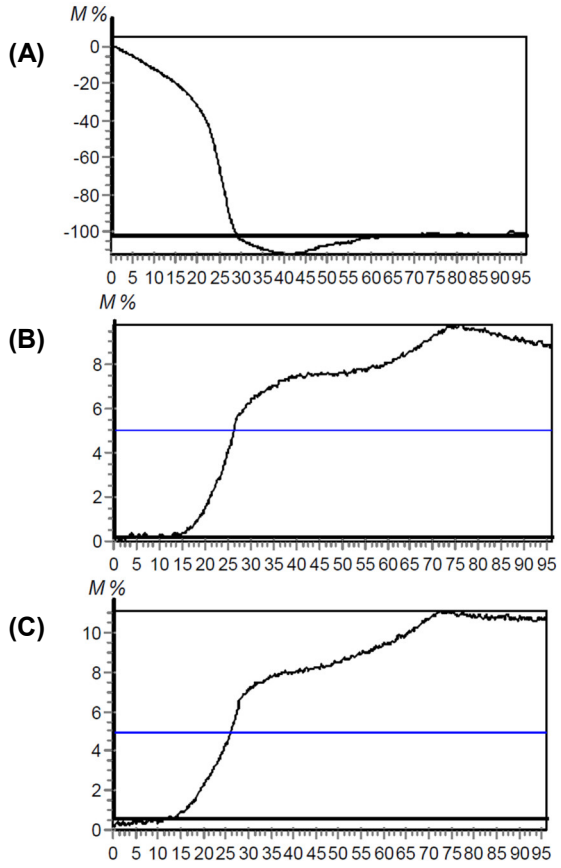

Figure 2. The results of three BacTrac measurements: relative changes in impedancy in the M% of media *vs.* time (h) - (A) indirect-; (B) aerobic-direct-; (C) anaerobic-direct measurements.

an incorporated valve for gas release, an aerobic one, and an indirect one (*Fig.2*). Only M% values yielded explainable curves. Indirect measurements yielded an inverse growth curve (decreasing) as expected, but did not exhibit a two-step decrease, i.e. diauxic growth, therefore, M% values of direct measurements were evaluated. The two curves of aerobic and anaerobic M% values were very similar to each other, but perhaps the anaerobic example is more relevant as in the case of high sugar content, the metabolism of yeast shifted in the anaerobic direction. *Fig.3* shows the fits of the model in which less constants had to be changed and diauxic growth was detected.

4. Conclusion

Both tested systems – Personal Bioreactor (RTS-1, Biosan) and BacTrac (SY-LAB) – detected diauxic cell growth of baking yeast. RTS-1 seemed to be a little bit more flexible, but BacTrac gave faster results, was able to make 40 measurements at the same time and offered three options in terms of evaluation. Maybe in the near future a solution to regular automatic sampling from

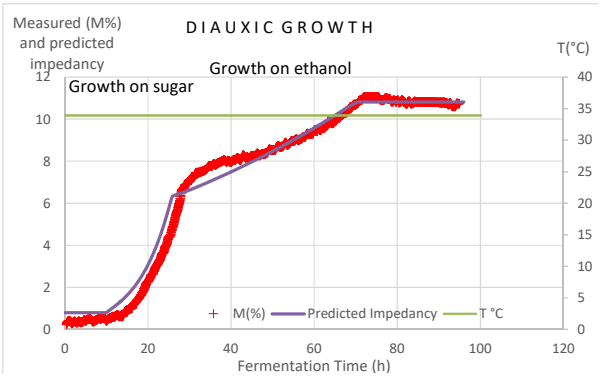

Figure 3. Model fitting to the anaerobic BacTrac curve (M%): red crosses: measured data; purple line: model-predicted values; green line: temperature (°C).

larger-scale fermenters will be found and then the results can be compared with the ones presented here.

Acknowledgement

We are sincerely grateful to SY-LAB for the support provided with regard to BacTrac, and to Biocenter Kft. for importing RTS-1.

REFERENCES

[1] Németh, Á.; Kiss, Á.; Sevella, B.: Experiments for D-lactic acid production with fermentation, *Hung. J. Ind. Chem.,* 2011 **39**(3), 359–362

[2] Bankovsky, V.; Bankovsky, I.; Bankovsky, P.; Isakova, J.; Djackova, I.; Sharipo, A.; Eskin, J.; Dišlers, A.; Rozenstein, R.; Saricev, V.; Djacenko, S.; Makarenko, V.; Balodis, U.: Reverse–Spin® Technology - Innovative Principle of Microbial Cultivation, Manufacturer's online leaflet: https://biosan.lv/images/uploads/content/files/reverse_spinner.pdf

[3] Blanch, H.W.; Clark, D.S.: Biochemical Engineering (Marcel Dekker, NY, USA), 1996, pp. 231–236 ISBN 9780824700997

DE GRUYTER

HUNGARIAN JOURNAL OF INDUSTRY AND CHEMISTRY
Vol. 45(2) pp. 23–27 (2017)
hjic.mk.uni-pannon.hu
DOI: 10.1515/hjic-2017-0016

HUNGARIAN JOURNAL OF INDUSTRY AND CHEMISTRY
HJIC

THE EFFECT OF ADVANCED OXIDATION PRE-TREATMENT ON THE MEMBRANE FILTRATION PARAMETERS OF DAIRY WASTEWATER

MIHÁLY ZAKAR,[1,2] ILDIKÓ KOVÁCS,[1] PÉTER MUHI,[1] ERIKA HANCZNÉ LAKATOS,[2] GÁBOR KESZTHELYI-SZABÓ,[1] ZSUZSANNA LÁSZLÓ[1,*]

[1] Institute of Mechanical and Process Engineering, Faculty of Engineering, University of Szeged, Moszkvai krt. 9, Szeged, 6724, HUNGARY
[2] Institute of Food Sciences, Széchenyi István University, Lucsony u. 15-17, Mosonmagyaróvár, 9200, HUNGARY

The dairy industry generates wastewater characterised by high levels of biological and chemical oxygen demands representative of their high degree of organic content; mainly carbohydrates, proteins and fats that originate from milk. Several investigations have been conducted into the reuse of dairy wastewater, e.g. membrane processes are a promising method to treat such wastewater. Earlier works have proven that with membrane filtration an appropriate degree of retention can be achieved and the permeate can be reused. However, membrane fouling is a limiting factor in these processes. Advanced oxidation processes (AOPs) are widely used in the fields of water and wastewater treatments and are known for their capability to mineralise a wide range of organic compounds. AOPs also exhibit some other effects on the filtration process, e.g. the microflocculation effect of ozone may play a significant role in increasing the elimination efficiency and causing a decreased level of irreversible fouling. By comparing ozone and Fenton pre-treatment (FPT) processes it can be shown that the fouling propensity of pre-treated pollutants does not depend on the pre-treatment method, while FPT was proven to be more efficient in improving the level of flux.

Keywords: ultrafiltration, ozone pre-treatment, Fenton-reaction, fouling resistances, dairy wastewater

1. Introduction

The dairy industry is considered to be the largest source of food-processing wastewater in many countries. Dairy wastewater exhibits high degrees of biological oxygen demand (BOD) and chemical oxygen demand (COD); contains high levels of dissolved or suspended solids including fats, oils and grease; as well as nutrients such as ammonium ions or phosphates. Therefore, proper attention must be paid to them before disposal [1]. There are several research projects that aim to identify possibilities of reusing or recycling dairy wastewater [2-9]. Membrane treatment of dairy wastewater with the aim of water reuse could simultaneously lower the total water consumption and effluent production of dairy plants, as the purified water produced could be reused in a dairy plant to heat or cool water. Besides additional advantages, e.g. a high degree of separation efficiency in the absence of chemical changes and low levels of energy intensity, membrane filtration also has drawbacks, namely compounds in dairy wastewater that contain protein were found to be significant foulants in terms of existing membrane materials [10-12].

The combination of membrane separation and pre-treatment with advanced oxidation processes (AOPs: using ozone, hydrogen peroxide, UV light, or a combination of these) opens up new opportunities, since the ozone and the resulting oxidizing radicals (mainly hydroxyl radicals) efficiently change the characteristics of the colloidal particles or oxidizing compounds, which cause membrane fouling [13]. Earlier studies have shown that the microflocculation effect of ozone may play a significant role in increasing the elimination efficiency and may decrease the extent of membrane fouling and increase the degree of gel formation. In addition, AOPs can be used as a pre-treatment stage before a biological step in order to increase the biodegradability of the recalcitrant compounds and thus lower the toxicity of the wastewaters [13-14].

According to economic evaluation studies, the Fenton process is more economical than ozone pre-treatment [15]. However, there is little data concerning its effect on membrane filtration parameters. The aim of the present work was to investigate and compare the effect of ozone pre-treatment and the Fenton's reaction on ultrafiltration parameters, fouling mechanisms and the pollutant removal efficiency on a model dairy wastewater.

*Correspondence: zsizsu@mk.u-szeged.hu

2. Experimental

2.1. Samples and Measurements

Model solutions were prepared from milk powder (Milk Quick, Instantpack Kft., Hungary) composed of 0.3% (g/g) concentrations, 32% (g/g) proteins, 5% (g/g) fat and 50% (g/g) lactose. Ozone was produced from oxygen (Linde, 3.0) with a flow-type ozone generator (Ozomatic Modular 4, Wedeco Ltd., Germany). The ozone-containing gas was bubbled continuously through a batch reactor during the treatment. The volume of the treated water was 0.45 dm^3. The durations of the treatment were 5, 10 and 20 mins; and the flow rate was 1 dm^3 min^{-1}. The ozone concentrations of the bubbling gas before and after it was passed through the batch reactor were measured with a ultraviolet–visible (UV-VIS) spectrophotometer (Nanocolor NUV 0113) at a wavelength of 254 nm (*Fig.1*). The absorbed ozone concentrations were $6.8 \cdot 10^{-4}$ M, $1.43 \cdot 10^{-3}$ M and $2.67 \cdot 10^{-3}$ M, respectively.

Fenton's reaction was conducted in a batch stirred ultrafiltration cell with 1.5 mmol dm^{-3} $FeSO_4 \times 7H_2O$ (purity 99%, Spektrum-3D, EU) adjusted to pH 3 with H_2SO_4 (purity 96%, Farmitalia Carlo Erba SPA, Italy), 0.3 wt.% milk powder solution and H_2O_2 solution (30%, purity 99%, Spektrum-3D Kft.), the $[H_2O_2]$:[Fe] ratio was 5:1 (Fenton (5:1)) or 50:1 (Fenton (50:1)). The ozone or Fenton pre-treated samples were used as a feed in ultrafiltration (UF) experiments.

The UF experiments were carried out in a batch stirred ultrafiltration cell (Millipore, Serial N°94, USA) with a capacity of 50 cm^3, and the filtrations were performed at transmembrane pressures of 0.1 (only in the case of Fenton (50:1)) or 0.3 MPa and the feed solutions were stirred at 350 rpm. For filtration experiments, flat sheet polyethersulfone (PES) membranes (PES-10 series, New Logic Research Inc., USA) and a molecular weight cut-off (MWCO) of 10 kDa were used with an effective membrane surface area of 1.73 dm^2. The initial feed volume was 50 cm^3, the ultrafiltration experiments were conducted until 40 cm^3 of the total sample had been filtered, when the volume reduction ratio (VRR) was equal to 5.

Determination of the COD was based on the standard method involving the oxidation of potassium dichromate; for the analysis, standard test tubes (Lovibond Tintometer Ltd.) were used. The digestions were conducted in a COD digester (Lovibond ET108 thermoreactor); and the COD values were measured with a COD photometer (Lovibond PCCheckit). For the determination of the residual amount of hydrogen peroxide, COD measurements were performed before and after the addition of the enzyme catalase.

2.2. Theoretical Methodologies

In order to investigate mechanisms of membrane fouling, filtration resistances were calculated according to the Resistance-In-Series Model, *Eqs.(1-4)*.

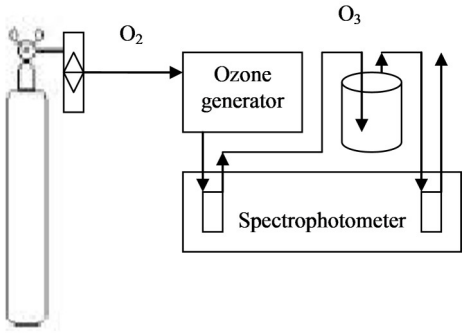

Figure 1. Experimental set-up of ozonation.

The membrane resistance (R_M , m^{-1}) was calculated as

$$R_M = \frac{\Delta p}{J_w \eta_w} \quad [m^{-1}] \tag{1}$$

where Δp is the difference in pressure either side of the membrane (in MPa), J_w is the water flux of the clean membrane, and η_w is the viscosity of water (in Pa·s).

The total resistance (R_T , in m^{-1}), can be evaluated from the steady-state flux by using the Resistance-In-Series Model:

$$R_T = R_M + R_{irrev} + R_{rev} \tag{2}$$

where R_{irrev} is the irreversible resistance (mainly caused by the fouled pores) and R_{rev} is the reversible resistance.

The irreversible resistance was determined by measuring the water flux through the membrane after filtration, rinsing it with deionized water to remove any particles of the residue layer from the surface, and subtracting the resistance of the clean membrane:

$$R_{irrev} = \frac{\Delta p}{J_{WA} \eta_W} - R_M \tag{3}$$

where J_{WA} is the water flux after concentration tests. The reversible resistance of the layer deposited on the membrane surface was calculated as:

$$R_{rev} = \frac{\Delta p}{J_C \eta_{WW}} - R_{irrev} - R_M \tag{4}$$

where J_C is the constant flux at the end of the concentration test and η_{WW} is the viscosity of the wastewater viscosity [16].

Mathematical modelling of the fouling mechanism was studied based on the Hermia's model [17]. The Hermia's model describes the mechanism of membrane fouling based on blocking filtration laws, consisting of complete pore blocking, standard pore blocking and intermediate pore blocking, in addition to cake filtration (*Table 1*) to illustrate the different fouling mechanisms.

Table 1. Hermia's filtration laws.

Fouling mechanism	Filtration law	Constant-pressure filtration $J_0 A$ = cont.
Complete pore blocking	$J = J_0 e^{-kt}$	$\ln J = \ln J_0 - kt$
Gradual pore blocking (standard pore blocking)	$J = J_0 \cdot (1 + ½ K_s (A \cdot J_0)^{½} \cdot t)^{-2}$	$1/J^{0.5} = 1/J_0^{0.5} + k_s \cdot t$ $k_s = 0.5 K_s A^{0.5}$
Intermediate filtration	$J = J_0 \cdot (1 + K_i \cdot A \cdot J_0 \cdot t)^{-1}$	$1/J = 1/J_0 + k_i \cdot t$ $k_i = K_i A$
Cake filtration	$J = J_0 \cdot (1 + 2K_c (A \cdot J_0)^2 \cdot t)^{-0.5}$	$1/J^2 = 1/J_0^2 + k_c \cdot t$ $k_c = 2K_c A^2$

The Hermia's model was then linearized for each model using a fitting equation in terms of the permeate flux versus time as presented in *Table 1*. In terms of the evaluation of the results these models were fitted to experimental data. In *Table 1*, J is the flux, J_0 is the initial flux, the various K's are the fouling coefficients, and A is a constant.

To compare the performance of different AOPs, the oxygen-equivalent chemical-oxidation capacity (OCC, kg O_2 m^{-3}) was used to quantify the oxidants used in the ozone treatment and Fenton's reaction, and was determined based on stoichiometric calculations [14]:

$$OCC = 1.000[O_3] = 0.471[H_2O_2] \quad (5)$$

where $[O_3]$ is the required ozone concentration (kg O_3 m^{-3}), and $[H_2O_2]$ is the required hydrogen peroxide concentration (kg H_2O_2 m^{-3}).

3. Results and Analysis

3.1. Experiments

The effect of pre-oxidation on filtration parameters was investigated by fitting equations in *Table 1* to measured data. Based on the value of the coefficient of determination, the cake layer filtration yielded the best correlation. In order to compare the different pre-oxidation methods, normalised values of the initial flux (J_0, L m^{-2} h^{-1} bar^{-1}) and fouling coefficients (k) were calculated and compared (*Figs.2* and *3*). It was found that the effect of ozone treatment and Fenton-treatment is different in the case of initial normalised flux. Not only the Fenton pre-treatment but the addition of reagents in the absence of hydrogen peroxide exhibited coagulation-flocculation effects that resulted in an enhanced initial flux. In the case of the Fenton's reaction this effect is independent of the $[H_2O_2]$:[Fe] ratio.

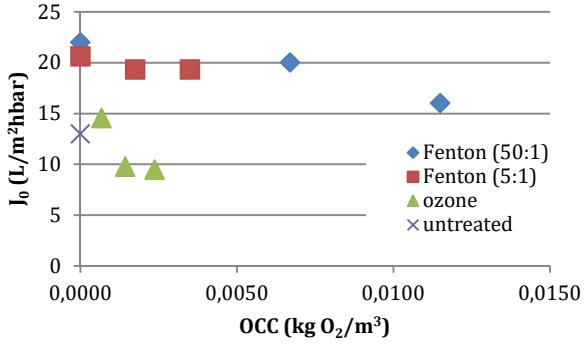

Figure 2. Normalised initial flux values as a function of OCC.

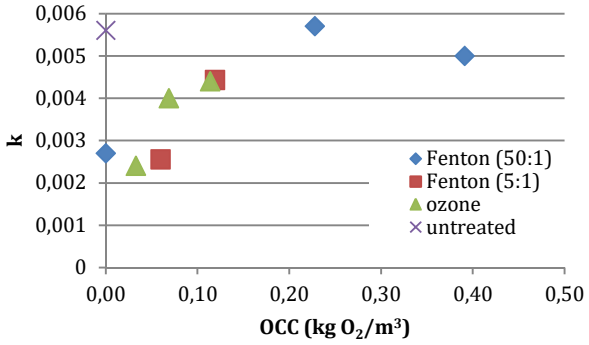

Figure 3. Fouling coefficient as a function of OCC.

The fouling coefficient also changes by the addition of oxidants, (*Fig.3)* but in this case, the tendency is more likely to depend on the OCC than on the applied AOP method. At lower oxidation capacities the fouling coefficient decreases resulting in lower degrees of fouling than in non-treated solutions, however, at higher oxidation grades, the fouling coefficient increases.

To obtain more information concerning the fouling mechanisms, the filtration resistances of ozone-treated and Fenton (5:1) pre-treated solutions were calculated and compared (*Fig.4*). It was found that - in accordance with the values of the fouling coefficient - filtration resistances decrease as the duration of oxidation pre-treatment increases. In particular, mainly pre-treatments of short durations decreased the irreversible fouling resistance and increased the reversible fouling resistance.

4. Discussion

As an effect of the pre-oxidation of model dairy wastewater two typical pathways were observed that influence membrane filtration parameters: the i) micro-

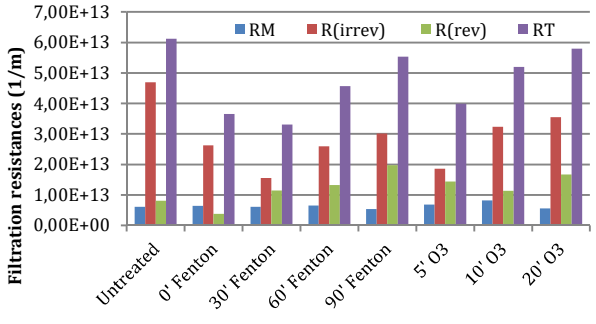

Figure 4. Filtration resistances of untreated, Fenton (5:1) and ozone pre-treated solutions.

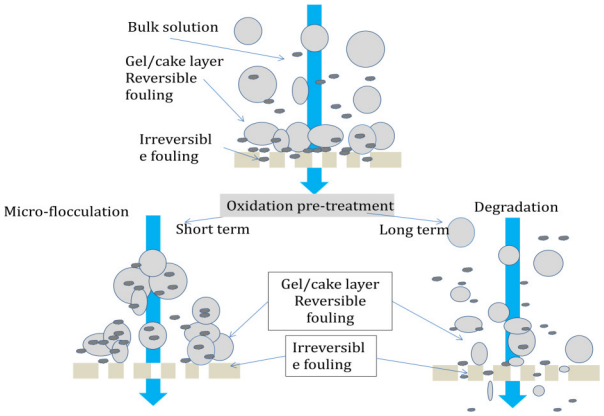

Figure 5. Possible effect of ozone pre-treatment on the membrane filtration of dairy wastewater.

flocculation effect produces associated colloidal particles, and ii) degradation of organic matter (*Fig.5*). The former resulted in decreased fouling of membrane pores as shown by the decreased fouling coefficient and irreversible resistance. This can be observed only during short-term ozone or Fenton treatments (OCC < 0.05 kg O_2 m^{-3}). The latter point may increase the degree of pore fouling [13, 18] due to the formation of small degradation by-products, which can enter membrane pores as the increased values of irreversible resistance also prove. By comparing the ozone and Fenton pre-treatment processes with similar OCCs, it can be concluded that the Fenton pre-treatment may be more effective in terms of enhancing the flux, probably due to the coagulation-flocculation effect of the ferrous salts themselves.

5. Conclusion

The comparison of ozone and Fenton processes as pre-treatments before ultrafiltration of a model sample of dairy wastewater showed that such pre-treatments may improve the filtration parameters in terms of flux or fouling mitigation. By examining the effect of the oxidation capacities of ozone and Fenton pre-treatment processes, it was found that the fouling propensity of pollutants does not depend on the pre-treatment method. However, it depends on the OCC of the pre-treatment method. Although the method of pre-treatment affects the flux, the Fenton pre-treatment proved to be more efficient in terms of enhancing the value of the flux.

SYMBOLS

R_M	membrane resistance (m^{-1})
R_{rev}	reversible resistance (m^{-1})
R_{irrev}	irreversible resistance (m^{-1})
Δp	pressure difference between the two sides of the membrane (MPa)
J	flux (1/s)
J_W	water flux (1/s)
J_C	constant flux at the end of the concentration (1/s)
J_0	initial flux (1/s)
η_W	water viscosity (Pa·s)
k	fouling coefficient
OCC	oxygen-equivalent chemical-oxidation capacity (kg $O_2 \cdot m^{-3}$)

Acknowledgement

This research was supported by the János Bolyai Research Fellowship of the Hungarian Academy of Sciences. The authors are also grateful for the financial support of the National Research, Development and Innovation Office (NKFIH K112096).

REFERENCES

[1] Farizoglu, B.; Uzuner, S.: The investigation of dairy industry wastewater treatment in a biological high performance membrane system, *Biochem. Eng. J.*, 2011 **57**, 46–54 DOI: 10.1016/j.bej.2011.08.007

[2] Vourch, M.; Balance, B.; Chaufer, B.; Dorange, G.: Treatment of dairy industry wastewater by reverse osmosis for water reuse, *Desalination*, 2008 **219**(1-3), 190–202 DOI 10.1016/j.desal.2007.05.013

[3] Perle, M.; Kimchie, S.; Shelef, G.: Some biochemical aspects of the anaerobic degradation of dairy wastewater, *Water Res.*, 1995 **29**(6), 1549–1554 DOI 10.1016/0043-1354(94)00248-6

[4] Bick, A.; Plazas, T.J.G.; Yang, F.; Raveh, A.; Hagin, J.; Oron, G.: Immersed Membrane Bio Reactor (IMBR) for treatment of combined domestic and dairy wastewater in an isolated farm: An exploratory case study implementing the Facet Analysis (FA), *Desalination*, 2009 **249**(3), 1217–1222 DOI 10.1016/j.desal.2009.06.035

[5] Sarkar, B.; Chakrabarti, P.P.; Vijaykumar, A.; Kale, V.: Wastewater treatment in dairy industries: possibility of reuse, *Desalination*, 2006 **195**(1-3), 141–152 DOI 10.1016/j.desal.2005.11.015

[6] Andrade, L.H.; Motta, G.E.; Amaral, M.C.S.: Treatment of dairy wastewater with a membrane bioreactor, *Braz. J. Chem. Engng.*, 2013 **30**(4), 759–770 DOI 10.1590/S0104-66322013000400008

[7] Yip, V.; Arntfield, S.D.; Hydamaka, A.W.: Potential for stainless steel microfiltration processing to reduce effluent from a fluid milk and ice-cream processing plant, *J. Dairy Sci.*, 1996 **79**(4), 710–716 DOI 10.3168/jds.S0022-0302(96)76417-2

[8] Koyuncu, I.; Turan, M.; Topacik, D.; Ates, A.: Application of low pressure nanofiltration membranes, for the recovery and reuse of dairy industry effluents, *Water Sci. Tech.*, 2000 **41**(1) 213–221 web: http://wst.iwaponline.com/content/41/1/213

[9] Luo, J.; Ding, L.; Qi, B.; Jaffrin, M.Y.; Wan, Y.: A two-stage ultrafiltration and nanofiltration process for recycling dairy wastewater, *Bioresour. Technol.*, 2011 **102**(16), 7437–7442 DOI 10.1016/j.biortech.2011.05.012

[10] Bégoin, L.; Rabiller-Baudry, M.; Chaufer, B.; Faille, C.; Blanpain-Avet, P.; Bénézech, T.; Doneva, T.: Methodology of analysis of a spiral-wound module. Application to PES membrane for ultrafiltration of skimmed milk, *Desalination*, 2006 **192**(1-3), 40–53 DOI 10.1016/j.desal.2005.10.010

[11] Koutake, M.; Uchida, Y.; Sato, T.; Shimoda, K.; Watanabe, A.; Nakao, S.: Filtration membrane fouling in ultrafiltration of skim milk, 1: Causes and cleaning, *J. Agric. Chem. Soc. Jpn.*, 1987 **198**, 677–681 web: http://agris.fao.org/agris-search/search.do?recordID=JP880163288

[12] Rabiller-Baudry, M.; Le Maux, M.; Chaufer, B.; Begoin, L.: Characterisation of cleaned and fouled membrane by ATR-FTIR and EDX analysis coupled with SEM: Application to UF of skimmed milk with a PES membrane, *Desalination*, 2002 **146**(1-3), 123–128 DOI 10.1016/S0011-9164(02)00503-9

[13] László, Zs.; Kertész, Sz.; Beszédes, S.; Hovorka-Horváth, Zs.; Szabó, G.; Hodúr, C.: Effect of preozonation on the filterability of model dairy waste water in nanofiltration, *Desalination*, 2009 **240**(1-3), 170–177 DOI 10.1016/j.desal.2007.12.040

[14] Cańizares, P.; Paz, R.; Sáez, C.; Rodrigo, M.A.: Costs of the electrochemical oxidation of wastewaters: a comparison with ozonation and Fenton oxidation processes, *J. Environ. Mgmt.*, 2009 **90**(1), 410–420 DOI 10.1016/j.jenvman.2007.10.010

[15] Özge, S.; Taner, Y.: Determination of the acute toxicities of physicochemical pretreatment and advanced oxidation processes applied to dairy effluents on activated sludge, American Dairy Science Association, *J. Dairy Sci.,* 2015 **98**(4), 2337–2344 DOI 10.3168/jds.2014-8278

[16] Kertész, Sz.; László, Zs.; Forgács, E.; Szabó, G.; Hodúr, C.: Dairy waste-water purification by vibratory shear enhanced processing, *Desalination Water Treat.,* 2012 **37**(1-3), 1–7 DOI 10.5004/dwt.2011.2485

[17] Hermia, J.: Constant pressure blocking filtration law: Application to power law non-newtonian fluids, *Trans. Ind. Chem. Eng*., 1982 **60**(3), 183–187 web: http://hdl.handle.net/2078.1/57489

[18] Zhu, H.T.; Wen, X.H.; Huang, X.: Pre-ozonation for dead-end microfiltration of the secondary effluent: suspended particles and membrane fouling, *Desalination*, 2008 **231**(1-3), 166–174 DOI 10.1016/j.desal.2007.11.044

DE GRUYTER

HUNGARIAN JOURNAL OF
INDUSTRY AND CHEMISTRY
Vol. 45(2) pp. 29–33 (2017)
hjic.mk.uni-pannon.hu
DOI: 10.1515/hjic-2017-0017

HUNGARIAN JOURNAL OF INDUSTRY AND CHEMISTRY
HJIC

MICROENCAPSULATION OF VEGETABLE OIL: ALTERNATIVE APPROACHES USING MEMBRANE TECHNOLOGY AND SPRAY DRYING

KRISZTINA ALBERT,* GYULA VATAI, AND ANDRÁS KORIS

Department of Food Engineering, Szent István University, Ménesi út 44, Budapest, 1118, HUNGARY

Microencapsulation technology is a method that is widely used in the food industry. By comparing the latest encapsulation techniques, a significant number of publications concern membrane technology. The term "membrane-based encapsulation" entails that the first step of the technique is the preparation of emulsion with the help of microporous membranes. Generally, in microencapsulation technologies, the wall material is dissolved in a continuous phase and oil is dispersed within it. In the present investigation, a new method of preparing microcapsules composed of vegetable oil and maltodextrin was developed. In the first step, the wall material (maltodextrin) was dissolved in oil and considered as a dispersed phase, subsequently, it was introduced into a continuous phase (water) through a microporous membrane. A comparative study was conducted between conventional microencapsulation techniques and one developed in our laboratory. The average particle size of microcapsules prepared by our method is smaller than the size allowed by other methods. After encapsulation preparation, fine-tuned microcapsules were produced by spray drying. However, the main disadvantage of our proposed technology is rapid membrane fouling, because of high concentrations of solute in the dispersed phase. This problem can be eliminated by judicious and systematic investigations.

Keywords: vegetable oil, microencapsulation, membrane technology, spray drying

1. Introduction

The controlled release of food ingredients at the right place and the right time is a key functionality that can be provided by microencapsulation. In food products, fats and oils, aroma compounds, vitamins, minerals, colourants and enzymes are encapsulated.

The process of the encapsulation of sensitive compounds consists of two steps: the first is often emulsion production: emulsification of core materials with dense solutions of wall material; the second is drying or cooling of emulsion by some chemical or mechanical process; and at the end of these processes microparticles can be obtained [1]. The two major industrial encapsulation processes are spray drying and extrusion [2]. *Table 1* summarizes literature reviews that focus on these technologies, where the two steps of microencapsulation are performed by the combination of so-called membrane emulsification and spray drying.

Membrane emulsification (ME) is a relatively new, simple emulsion-production method which can be conducted with the use of a microporous membrane. Other emulsification processes within this category, besides ME and spray drying, include simple blending as well as homogenization; and secondary reactions that recover the capsules from the emulsion are interfacial polymerization, vacuum heat treatment, solvent diffusion and freeze drying. Different materials are used as the dispersed phase and wall materials of the microcapsules. The continuous phase is typically water.

*Correspondence: albert.krisztina@etk.szie.hu

2. Experimental

The main objective of this study was to initially prepare emulsions and form microcapsules using three different methods. The first approach was conventional membrane emulsification. The second one was conducted by a modified ME process. The third involved the use of a laboratory blender. In all three cases, the second step was the spray-drying technique to recover the microcapsules from the emulsions.

2.1. Samples and Measurements

All chemicals (maltodextrin, Tween-80 emulsifier) were procured from Shop.Builder, Hungary and Sigma-Aldrich, Germany. Commercial-grade sunflower-seed oil was purchased from a local market in the vicinity of Budapest.

2.2. Membrane Emulsification Apparatus

A cross-flow membrane emulsification system was used as the emulsification process (*Fig.1*). The apparatus included two manometers positioned at the opposite

Table 1. Summary of examples from the literature of microencapsulation technologies.

Emulsification	Secondary reaction	Dispersed phase / Wall material
membrane emulsification		oil / polyvinylpyrrolidone (PVP) [3]
	spray-drying	fish oil / whey protein isolate (WPI), whey protein hydrolysate (WPH), sodium caseinate, maltodextrin [4]
	interfacial polymerization	benzene, xylene, liquid paraffin / terephthaloyl dichloride (TDC) [5]
	vacuum heat treatment	oil / polyethersulphone (PES) [6]
	solvent diffusion	oil / polycaprolactone (PCL), dichloromethane (DCM) [7]
	freeze-drying	chloroform + curcumin / poly(lactic-co-glycolic acid) (PLGA) [8]
blending and homogenization	spray-drying	extra virgin olive oil / gelatin, gum arabic, starch, lactose, maltodextrin [9]
		olive oil + α-Tocopherol / maltodextrin, agave inulin, acacia gum [10]
		walnut and chia oil / maltodextrin, (hydroxypropyl)methyl cellulose [11]
		ginger oil / cashew gum, inulin [12]
		walnut oil / skimmed milk powder (SMP), SMP+Tween 80, SMP+maltodextrin [13]
		Nigella sativa oil / sodium caseinate, maltodextrin [14]
		chili seed oil / sodium octenylsuccinate starch, maltodextrin [15]
	freeze-drying	Ziziphora clinopodiodes essential oil / whey protein isolate (WPI), pectin [16]

ends of the membrane to measure the drop in pressure along the membrane. The pressure of the dispersed phase was guaranteed by compressed air from an air pump which was injected from the outer surface of the membrane. The continuous phase was recirculated on the lumen side of the membrane by a pump. A rotameter, placed at the exit of the membrane, allowed the flow rate of the continuous phase to be measured.

2.3. Microencapsulation Process

Microcapsules were prepared by a tubular ceramic membrane with a pore size of 1.4 μm (PALL Austria Filter GmbH). The membrane was composed of α-alumina and the surface area of the active membrane was 50 cm^2. Cross-flow operation was adopted for emulsion production. The first emulsion was prepared using a conventional membrane emulsification technique. The wall material (maltodextrin) was dissolved in the continuous phase (water) and sunflower-seed oil was dispersed into it. The direction of flow of the dispersed phase was tangential with the surface of the membrane. Otherwise, in the second case the wall material was mixed with sunflower-seed oil. This mixture was considered as the dispersed phase and it was pressed through the membrane pores under pressure. In both cases the pressure of the dispersed phase was 2.5 bars and the recirculation flow rate of the continuous phase was 150 $dm^3\ h^{-1}$. In the third case the emulsion was prepared at room temperature using a laboratory blender at 2,000 rpm for 40 minutes.

2.4. Spray Drying

The emulsions prepared were spray dried with a laboratory-scale spray dryer (LabPlant SD-05) equipped with a nozzle of 0.5 mm in diameter. The pressure of the compressed air in terms of the flow of the spray was adjusted to 3.6 bars. The air temperature at the inlet was maintained at 180±5 °C, and the feed rate was adjusted to 475 $cm^3\ h^{-1}$, respectively. Emulsions were prepared during the spray drying process and were continuously stirred by a magnetic stirrer throughout. The microcapsules were collected from the collecting chamber and stored in darkness until analysed.

2.5. Analysis of Microcapsules

Following the emulsion preparation, the average droplet size and span value were measured by a FRITSCH Laser Particle Sizer ANALYSETTE 22 NanoTec. Each sample was analyzed three times and the average data reported. The span value was considered as an indication of the dispersity of the droplet size. The lower the span value, the more monodisperse the emulsion. A VHX-6000 digital microscope manufactured by KEYENCE was used to check the formation of microcapsules and evaluate their morphology.

2.6. Surface-Oil Content and Microencapsulation Efficiency

The procedure modified by Calvo *et al.* [9] to determine the surface-oil content and microencapsulation efficiency was employed to measure the amount of unencapsulated oil present on the surface of the powders. Briefly, 5 g of microcapsules were precisely

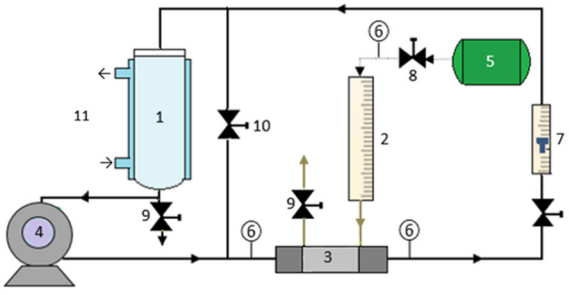

Figure 1. Experimental set-up for the cross-flow membrane emulsification process: (1) continuous phase tank, (2) graduated disperse phase tank, (3) membrane module, (4) pump, (5) compressor, (6) pressure meter, (7) rotameter, (8) pressure controller, (9) valve on drain, (10) valve, (11) heating / cooling (thermostat).

Table 2. Results of emulsification.

Conventional method using ME (1)	Droplet size = 9.18 μm Span = 1.5 Average flux = 368.36 $dm^3\ m^{-2}\ h^{-1}$
New method using ME (2)	Droplet size = 7.58 μm Span = 1.72 Average flux = 159.29 $dm^3\ m^{-2}\ h^{-1}$
Laboratory blender (3)	Droplet size = 7.12 μm Span = 1.88

weighed in a beaker and 50 cm^3 of hexane was added and shaken by hand for 15 s at ambient temperature to extract the superficial oil. The solvent mixture was then filtered through filter paper, and subsequently the unencapsulated oil was collected after evaporation of the hexane under a vacuum. To measure the total amount of encapsulated oil, the same procedure was conducted, but the powder of microcapsules in hexane as an extraction solvent was stirred for 4 h using a magnetic stirrer. For the production of microcapsules in oil, the encapsulation efficiency (*EE*) is an important parameter which is strongly related to the amount of oil on the surface, and was calculated using the following equation:

$$EE = \frac{\text{Total oil} - \text{Surface oil}}{\text{Total oil}} \times 100 \qquad (1)$$

3. Results and Analysis

The first part of this section presents the results in terms of the production of sunflower-seed oil/water emulsions by conventional and modified-membrane emulsification techniques using a laboratory blender, then the encapsulation efficiency and the physical characterization of the obtained microcapsules are presented.

3.1. Results of Emulsification

The results of particle-size measurements are summarized in *Table 2*. The average droplet sizes were 9.18 μm, 7.58 μm and 7.12 μm in the three different emulsification cases. The average droplet size of microcapsules prepared in the modified way, when the wall material was mixed with the dispersed phase, was lower than those prepared using the conventional technique.

In 2000, Joscelyne, along with his co-worker, reported that for membrane emulsification, the size of synthesized emulsion particles might be 2-10 times greater than the pore size of the membrane. The present investigators used a microporous membrane with a pore size of 1.4 μm and it was found that in all three cases the average size of the synthesized microcapsules is in line with the conclusion reached by a previously mentioned research group [17]. As an example, the shape and morphology of synthesized microcapsules prepared by the modified ME methods are shown in *Fig.2*.

Table 3. Oil encapsulation efficiency of microcapsules.

Conventional method with ME (1)	36.4 %
New method with ME (2)	34.5 %
Laboratory blender (3)	28.2 %

3.2. Spray-Drying Results

Sunflower-seed oil microcapsules were obtained by spray drying the oil-in-water (O/W) emulsions. The novelty of the approach adopted in the present study is that it utilizes membrane emulsification, which is a low-energy technology, to produce sunflower-seed oil/water emulsions stabilized by maltodextrin which has been dried by spray drying. The results, represented in *Table 3*, show that the encapsulation efficiency is enhanced by this modern method, the highest values correspond to microcapsules produced by this membrane technology. By comparing the encapsulation efficiency of microcapsules produced by conventional microencapsulation techniques with our laboratory-developed method, it should be mentioned that there is

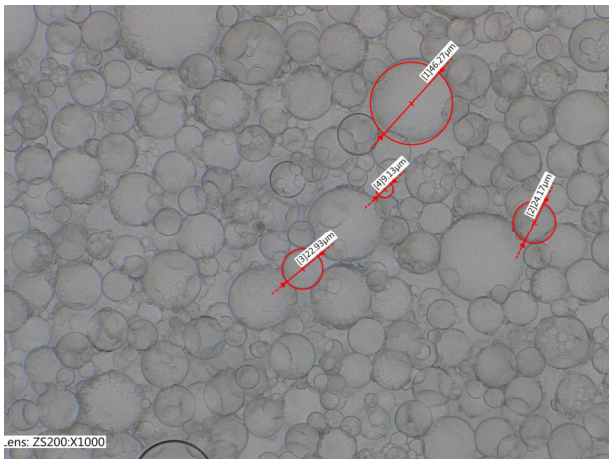

Figure 2. Microscopic image of emulsion sample at 1000× magnification.

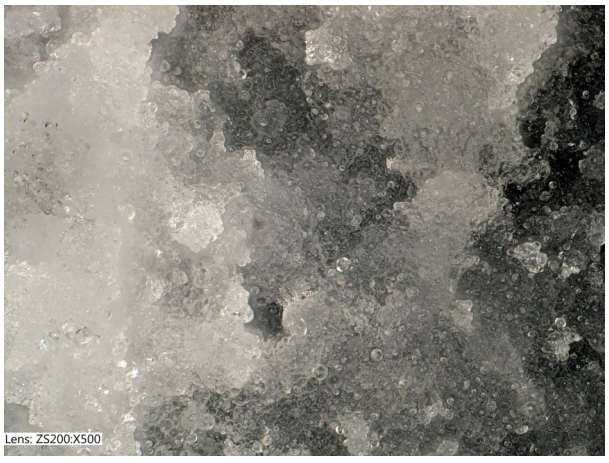

Figure 3. Image of microencapsulated sunflower-seed oil powder produced by conventional ME at 500× magnification.

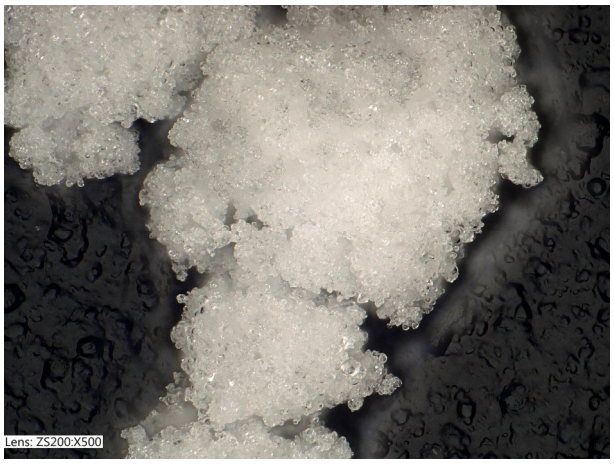

Figure 4. Image of microencapsulated sunflower-seed oil powder produced by modified ME at 500× magnification.

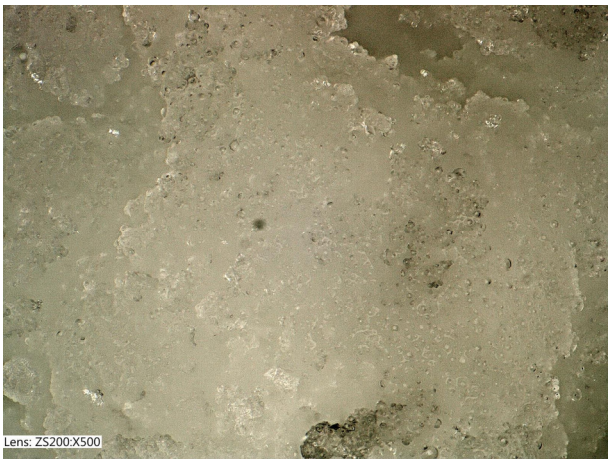

Figure 5. Image of microencapsulated sunflower-seed oil powder produced by a laboratory blender at 500× magnification.

no significant difference in terms of encapsulation efficiency.

The surface and external morphologies of the microcapsules of sunflower-seed oil were studied using optical microscopy *(Figs.3-5)*. In terms of particle morphology, the microstructures of the powders containing maltodextrin as a wall material were generally spherical in shape, homogeneous and exhibited a smooth surface as seen in the microscopic images. In 2015, Koç et al. [18] reported that the smooth surface of microencapsulated extra virgin olive oil using maltodextrin is related to the low-molecular-weight sugar content of maltodextrin. These low molecular weight sugars may act as plasticizers on the surface of the particles during spray drying. In their study, when WPI (whey protein isolate) was selected as the wall material, the particles exhibited a rough surface compared to those containing maltodextrin.

4. Conclusion

Our work focused on basic research in terms of microcapsule production under a laboratory set-up. The main aim of the present investigation was to gain experience with regard to the preparation of microcapsules by membrane emulsification in combination with spray drying using a novel technique and to compare it with the conventional one. The operation of the process and its basic correlations were the primary foci of this paper. Based on the results obtained it is possible to draw up experimental plans that refine and optimize the process. The results of this work demonstrate that a modified membrane emulsification technique, in which the wall material is mixed with the dispersed phase and not with the continuous phase, combined with spray drying can be used to produce microcapsules of sunflower-seed oil that possess an appropriate oil-encapsulation efficiency.

Acknowledgement

The authors acknowledge the financial support of the ÚNKP-16-3-III New National Excellence Program of the Ministry of Human Capacities. They would like to thank KEYENCE Magyarország for providing the microscopic images.

REFERENCES

[1] Madene, A.; Jacquet, M.; Scher, J.; Desobry, S.: Flavour encapsulation and controlled release – a review, *IJFST*, 2006 **41**(1), 1–21 DOI 10.1111/j.1365-2621.2005.00980.x

[2] Gouin, S.: Microencapsulation: industrial appraisal of existing technologies and trends, *TIFS*, 2004 **15**(7-8), 330–347 DOI 10.1016/j.tifs.2003.10.005

[3] Choi, H.G.; Yong, C.S.; Yang, K.Y.: Oral solid preparation composition containing silymarin using membrane emulsification technique, and its production method, 2010, KR20120034264

[4] Ramakrishnan, S.; Ferrando, M.; Güell, C.: Food grade microcapsules produced by membrane emulsification, *Procedia Engng.*, 2012 **44**, 1530–1533 DOI 10.1016/j.proeng.2012.08.855

[5] Chu, L.-Y.; Xie, R.; Zhu, J.-H.; Chen, W.-M.; Jamaguchi, T.; Nakao, S.-I.: Study of SPG membrane emulsification processes for the preparation of monodisperse core-shell microcapsules, *J. Colloid Interface Sci.,* 2003 **265**(1), 187–196 DOI 10.1016/S0021-9797(03)00350-3

[6] Figoli, A.; Shanthana Lakshmi, D.; Piacentini, E.; Giorno, L.; Drioli, E.: Preparation of novel ionic liquid loaded polymeric microspheres by membrane emulsification process, *Procedia Engng.,* 2012 **44**, 1287–1290 DOI 10.1016/j.proeng.2012.08.757

[7] Imbrogno, A.; Piacentini, E.; Drioli, E.; Giorno, L.: Preparation of uniform polycaprolactone microparticles by membrane emulsification/solvent diffusion process, *JMSC,* 2014 **467**, 262–268 DOI 10.1016/j.memsci.2014.05.037

[8] Ho, T.H.; Dao, T.P.T.; Nguyen, T.A.; Le, D.D.; Dang, M.C.: Cross-flow membrane emulsification technique for fabrication of drug-loaded particles, *Adv. Nat. Sci. Nanosci. Nanotechnol.*, 2013 **4**, 045008 1–6 DOI 10.1088/2043-6262/4/4/045008

[9] Calvo, P.; Hernández, T.; Lozano, M.; González-Gómez, D.: Microencapsulation of extra-virgin olive oil by spray-drying: Influence of wall material and olive quality, *Eur. J. Lipid Sci. Technol.*, 2010 **112**(8), 852–858 DOI 10.1002/ejlt.201000059

[10] Turchiuli, C.; Jimenez Munguia, M.T.; Hernandez Sanchez, M.; Cortesferre, H.; Dumoulin, E.: Use of different supports for oil encapsulation in powder by spray drying, *Powder Technol.,* 2014 **255**, 103–108 DOI 10.1016/j.powtec.2013.08.026

[11] Martínez, M.E.; Curti, M.I.; Roccia, P.; Llabot, J.M.; Penci, M.C.; Bodoira, R.M.; Ribotta, P.D.: Oxidative stability of walnut (*Juglans regia L.*) and chia (*Salvia hispanica L.*) oils microencapsulated by spray drying, *Powder Technol.*, 2015 **270**, 271–277 DOI 10.1016/j.powtec.2014.10.031

[12] Fernandes, R.V.; Botrel, D.A.; Silva, E.K.; Borges, S.V.; Oliveira, C.R.; Yoshida, M.I.; Feitosa, J.P.; de Paula, R.C.: Cashew gum and inulin: new alternative for ginger essential oil microencapsulation, *Carbohydrate Polym.*, 2016 **153**, 133–142 DOI 10.1016/j.carbpol.2016.07.096

[13] Shamaei, S.; Seiiedlou, S.S.; Aghbashlo, M.; Tsotsas, E.; Kharaghani, A.: Microencapsulation of walnut oil by spray drying: Effects of wall material and drying conditions on physicochemical properties of microcapsules, *IFSET,* 2017 **39**, 101–112 DOI 10.1016/j.ifset.2016.11.011

[14] Mohammed, N.K.; Tana, C.P.; Manap, Y.A.; Alhelli, A.M.; Hussin, A.S.M.: Process conditions of spray drying microencapsulation of *Nigella sativa* oil, *Powder Technol.*, 2017 **315**, 1–14 DOI 10.1016/j.powtec.2017.03.04

[15] Wang, Y.; Liu, B.; Wen, X.; Li, M.; Wang, K.; Ni, Y.: Quality analysis and microencapsulation of chili seed oil by spray drying with starch sodium octenylsuccinate and maltodextrin, *Powder Technol.,* 2017 **312**, 294–298 DOI 10.1016/j.powtec.2017.02.060

[16] Hosseinnia, M.; Khaledabad, M.A.; Almasi, H.: Optimization of *Ziziphora clinopodiodes* essential oil microencapsulation by whey protein isolate and pectin: a comparative study, *Int. J. Biol. Macromol.,* 2017 **101**, 958–966 DOI 10.1016/j.ijbiomac.2017.03.190

[17] Joscelyne, S.M.; Tragardh, G.: Membrane emulsification – a literature review, *JMSC,* 2000 **169**(1), 107–117 DOI 10.1016/S0376-7388(99)00334-8

[18] Koç, M.; Güngör, Ö.; Zungur, A.; Yalçin, B.; Selek, İ.S.; Ertekin, F.K.; Ötles, S.: Microencapsulation of extra virgin olive oil by spray drying: Effect of wall materials composition, process conditions, and emulsification method, *Food Bioprocess Technol.,* 2015 **8**, 301–318 DOI 10.1007/s11947-014-1404-9

DE GRUYTER

HUNGARIAN JOURNAL OF INDUSTRY AND CHEMISTRY
Vol. 45(2) pp. 35–39 (2017)
hjic.mk.uni-pannon.hu
DOI: 10.1515/hjic-2017-0018

HUNGARIAN JOURNAL OF INDUSTRY AND CHEMISTRY
HJIC

EFFECT OF CHAIN LENGTH AND ORDER OF THE ALCOHOL ON ENZYME ACTIVITY DURING ENZYMATIC ESTERIFICATION IN ORGANIC MEDIA

ZSÓFIA MÁRKUS, KATALIN BÉLAFI-BAKÓ, GÁBOR TÓTH, NÁNDOR NEMESTÓTHY AND LÁSZLÓ GUBICZA*

Research Institute on Bioengineering, Membrane Technology and Energetics, University of Pannonia, Egyetem u. 10, Veszprém, 8200, Hungary

Esters of short chain acids and alcohols are found in nature as compounds of flavors. Lately the method for their manufacture has been the enzymatic esterification in non-conventional media. Although several reactions have been studied in various media (organic solvents, ionic liquids, supercritical fluids, solvent-free systems), there has been no systematic investigation to clarify the effects of chain length and order of alcohols on the activity of the enzyme. In this work acetic acid was used as an acyl donor and the roles of the linear and branched chains of C_2-C_8 primary, secondary and tertiary alcohols on the activity of Novozym 435, the widely used lipase preparation were studied. Both the length of the carbon chain and the order of the alcohol were found to strongly influence the activity of the enzyme using the same operational parameters for the reactions. As a result of this project general conclusions were made with regard to the characters of alcohols affecting the reaction rates, which can be applied to other similar reactions.

Keywords: enzymatic esterification, non-conventional media, effect of alcohol chain lengths, lipase activity

1. Introduction

Enzyme technology provides a promising solution for the biosynthesis of natural flavor esters, since several enzymes are able to catalyze the synthesis of aroma compounds from precursor molecules [1]. Nowadays most flavor compounds are manufactured by conventional methods: chemical synthesis or recovery from natural sources. Esters produced chemically are quite common, but their method of production is not considered environmentally safe and cannot be classed as "natural". Recently interest has been growing in the production of these components by biotransformation, that is the manufacture of natural flavor esters by using natural raw materials. Lipases belong to the most diverse class of enzymes, they catalyze various reactions due to their wide spectrum of industrial applications. Lipase enzymes have been applied in many industrial sectors, e.g. the food and pharmaceutical industries, in the production of biological detergents (esters of carbohydrates), moreover in the manufacture of certain cosmetics and fragrances. Recently interest has grown in the production of natural flavor esters by the biosynthesis of short chain acids and alcohols [2,3].

Several similar reactions have been studied, most of which focused on the synthesis of acetates, like ethyl [4], butyl [5], hexyl [3], cinnamyl [6], and benzyl [7] acetates.

During the investigation of the reactions' parameters the roles of temperature, the molar ratio of acid to alcohol and the amount of enzyme were described in almost every paper. From these data the optimal values of these parameters could be estimated. Numerous reactions were carried out in organic solvents [8, 9], ionic liquids [10, 11], supercritical fluids (mainly in supercritical carbon dioxide) [12], solvent-free systems [13], in addition to in the gas phase [14]. Since these reactions can be conducted in non-aqueous media, the water content, to be more precise the water activity of the reaction mixture plays an extremely important role in terms of the reaction rate. For the operation of the enzyme lipase it is necessary to provide a minimal amount of water. On the other hand it is an equilibrium reaction, thus the greater excess of water shifts the reaction towards hydrolysis, decreasing the conversion rate significantly. The investigation of the effect of water content, or at least an intention to adjust the initial water content by a constant value is missing in several papers. The water content during the reaction continuously changes due to the production of water in the esterification. This effect can be neglected during the investigation of the initial reaction rates, but in terms of the development of continuous production it should be taken into account. A number of methods are known to maintain water content/activity. From a practical point of view membrane separation processes, like pervaporation provide attractive procedures [15].

*Correspondence: gubiczal@almos.uni-pannon.hu

Beyond the parameters mentioned and the water content, only a limited attention was paid to the role of substrates present in the reaction. As pointed out earlier, acetic acid was the acidic component used in most cases. The alcohols applied, however, were much more diverse: linear and branched chains, aromatic and different orders of alcohols were investigated. Nevertheless our group has not found a single study in the literature where *systematic* research was conducted to assess the role of alcohols on enzyme activity.

The effect of the chain length of various alcohols was investigated in reactions catalyzed by enzymes in non-conventional media. Romero and colleagues conducted experiments in supercritical carbon dioxide using four different alcohols: propanol, butanol, pentanol and octanol. It was found that higher degrees of conversion could be obtained by applying longer chain alcohols. Enzymes have a higher affinity towards longer chain alcohols, the difference, however, was small [16].

In another paper Romero used butyric acid as an acyl donor and the enzyme Novozym 435. An insignificant difference was observed in terms of the reaction rate or conversion during esterification when the four primary alcohols (propanol, butanol, hexanol and octanol) were applied. Applying secondary alcohols, e.g. 2-hexanol, however, yielded higher reaction rate and conversion than was the case with 2-butanol [17].

Pan et al. studied how the chain length of alcohol compounds can influence the resolution reaction of mandelic acid. Using methanol, ethanol, butanol, heptanol and octanol it was found that the highest degree of enantioselectivity could be obtained by ethanol. Moreover the reaction was described as following Michaelis-Menten kinetics in all cases and the inhibition constant increased as the carbon chain go longer [18].

Varma and Madras investigated the esterification of propionic acid and three different alcohols by the enzyme Novozym 435 in supercritical carbon dioxide. Primary (isobutanol, isoamyl alcohol) and secondary alcohols (isopropyl alcohol) were used, as well. Based on the measurements, it was concluded that enzymatic esterification was faster with primary alcohols than with secondary alcohols, moreover a greater degree of conversion was achieved with isobutanol than with isoamyl alcohol [19].

Therefore the aim of this paper was to study the role of alcohols by the preparation of a given enzyme whilst maintaining the operation parameters as constants. The esterification primary, secondary and tertiary alcohols of C_2-C_8 carbon chain lengths were investigated to be able to draw general conclusions concerning the role of alcohol structure on reaction rate. For the measurements a popular immobilized lipase enzyme preparation, Novozym 435®, was used.

2. Experimental

2.1. Chemicals and Enzymes

All chemicals: acetic acid, ethanol, 1-propanol. 1-butanol and n-hexane (Merck), 1-pentanol, 2-pentanol tert-butanol (2-methylpropan-2-ol) and 1-hexanol (Sigma-Aldrich); 1-heptanol (BDH Chemicals); 1-octanol and isobutanol (2-methylpropan-1-ol) (Spektrum-3D); isoamyl alcohol (3-methylbutan-1-ol) (Molar Chemicals); and 2-propanol, 2-butanol, tert-amyl alcohol (2-methylbutan-2-ol) and toluene (Reanal) were of analytical grade. The water content of the chemicals varied greatly, that is why they were dewatered over a 3Å molecular sieve in the form of beads (Sigma-Aldrich).

The enzyme used was Novozym 435® from *Candida antarctica* lipase B, immobilized on a macroporous acrylic resin with a water content of 1-2% w/w, which was kindly provided as a gift by Novo Nordisk A/S, Denmark. According to their commercial product manual, its catalytic activity was 7000 PLU/g (propyl laurate units/gram).

2.2. Reaction and Analysis

Reactions were carried out in 50 mL Erlenmeyer flasks on a laboratory incubator shaker (IKA incubator shaker, KS 4000i) at 150 rpm and 50 °C. The typical reaction mixture contained acetic acid (0.5 mmol), alcohol (3.0 mmol), Novozym 435® lipase (60 mg) and n-hexane (20 mL). The reaction was commenced by adding the enzyme.

The gas chromatography (GC) analyses for the determination of ester concentrations were conducted by a HP 5890 A gas chromatograph, with an HP-FFAP column (Macherey-Nagel), split: 70 kPa, N_2: 19 cm^3/min, using a flame ionization detector (FID). Toluene was used as an internal standard, the changes in ester yield were followed during the reaction. Samples were taken after reaction times of 0.5, 1.0, 2.0 4.0 and 6.0 min. The water contents of the reaction mixtures were determined by a Mettler DL35 Karl Fisher titrator.

3. Results and discussion

Although several publications have presented results on the production of flavor esters, the optimal initial conditions suggested were quite different and a high degree of deviation was found among data in the literature. Firstly the average of the literature data was used for our preliminary experiments. Based on these figures the following initial parameters were applied: in the reaction mixture the molar ratio of acetic acid to alcohol was 1:6, and 20 ml of n-hexane, 20 mmol of toluene and 60 mg of the enzyme Novozym 435 were added to it.

Table 1. The effect of water content on ester yield in the esterification of acetic acid and isoamyl alcohol

Time (h)	0.0%	0.3%	0.5%	0.7%
	Ester yield (%)			
0	0.0	0.0	0.0	0.0
0.5	3.2	16.7	18.5	20.5
1	8.3	28.8	33.4	30.7
2	15.8	50.2	48.3	46.7
4	24.2	73.5	68.2	60.3
6	33.1	85.4	79.7	68.5

3.1. The effect of water content

Experiments had to be conducted to determine the correct water content since it could not be found in the literature. The esterification of acetic acid and isoamyl alcohol – a reaction that has been quite frequently studied – was investigated under the conditions mentioned earlier. During the measurements completely dried reaction mixtures (0 % w/w water content) were used and others adjusted the initial water content to the levels of 0.3, 0.5 and 0.7 % w/w by adding water. As can be seen from the data of *Table 1*, the reaction was extremely slow in the case of completely dried solvents and reagents – as was expected. The reaction rate began to rise when the water content grew slowly (and approached the optimal value) due to the water forming in the reaction.

Based on the experimental results an initial water content of 0.3 % w/w was applied to further measurements since this water concentration provided the highest yield. The yields of esterification after a reaction time of 4 h were presented in *Fig.1*, where the measurements were taken under the conditions given earlier, with an adjusted and the same initial water contents. The yields of esterification were sufficiently high to observe the differences caused by the different structures of alcohols, but saturation levels were not reached and the distinct amounts of water formed during the reaction did not affect such a tendency either.

3.2. Primary alcohols

Our study involved linear and branched alcohols with a chain length of C_2-C_8. As can be seen from *Fig.1* for primary alcohols, the yield increased as the length of the carbon chain grew. The effect of chain length was investigated by Romero using propanol, butanol, hexanol as well as octanol and a similar conclusion was drawn: acetic acid conversion was greater with alcohols of longer chain lengths, thus the yields of esterification were higher, as well [16].

As far as branched primary alcohols were concerned, the opposite trend was observed: the yield of esterification decreased as the chain length increased. At the beginning of the reactions the differences were only minor: only a difference of 3 % was observed in the yields in the cases of alcohols consisting of a carbon chain of 4 or 5. The behavior of isooctanol was especially interesting, because a significant drop in yield was observed compared to the other linear, 8-carbon-chain alcohols – a far smaller amount of ester was formed in the reaction mixture.

Table 2. Ester yields using secondary alcohols

Secondary alcohol	Ester yield after 4 h (%)
2-propanol	35.8
2-butanol	44.8
2-pentanol	50.5

3.3. Secondary alcohols

In this work three secondary alcohols: 2-propanol, 2-butanol and 2-pentanol were used. As presented in *Table 2*, an increase in ester yields was observed as the carbon chain length of secondary alcohols grew, as well. The values, however were not as high as for primary alcohols. Neji et al. observed a similar behavior when butanol and 2-butanol were used in the esterification reaction [20]. Although both alcohols could perform esterification, yields of esterification were 50 % lower for secondary alcohols.

3.4. Tertiary alcohols

Among tertiary alcohols tert-amyl alcohol and tert-butanol were used, however, the enzyme was not able to convert them into esters using acetic acid. From the literature, Stavarache et al. applied tertiary alcohols for transesterification in the production of biodiesel [21]. Similarly no activity was observed during their experiments, not even when using ultrasonic radiation.

3.5. Discussion of the experimental results

Although our experimental results did not reveal entirely general conclusions, which are valid in all cases, obvious relationships could be formulated for certain

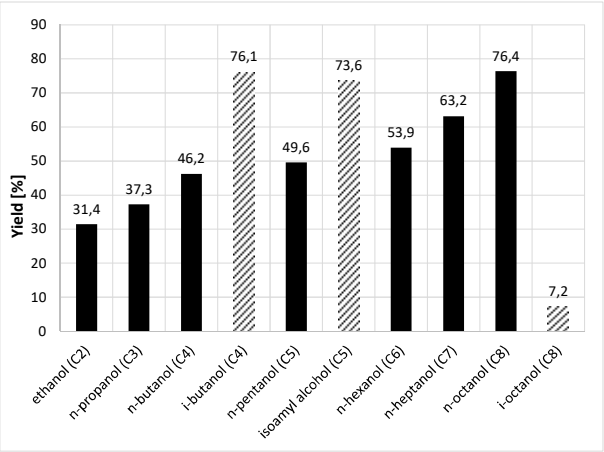

Figure 1. Ester yields during the reactions of acetic acid and primary alcohols after a reaction time of 4 h

groups of alcohols. It is certain that for alcohols with a linear carbon chain of C_2-C_8 in length, the conversion rate increases proportionally to the lengthening of the carbon chains. As for branched alcohols, the opposite tendency can be observed: yields were found to decrease as the carbon chain grew.

The relationship is more obvious when the order of alcohols is taken into consideration. Yields of esterification decreased in the following order: primary alcohol > secondary alcohol > tertiary alcohol (noting that tertiary alcohols did not react at all under the conditions used by Novozym 435). By applying other enzymes, e.g. carboxylesterase from *Bacillus licheniformis*, small degrees of conversion were measured, but remained close to the limit of detection [22]. In an attempt to justify such behavior, it can be assumed that access of the hydroxyl group of the alcohol to the active centre of the enzyme is severely sterically hindered in the case of secondary and especially tertiary alcohols, which cause enzyme activity to decline or even cease.

4. Conclusion

The expected reaction rate produced by a given enzyme can be predicted according to characteristics of the alcohol used, namely carbon chain length, linear or branched, and the order in production of flavor esters by enzymatic esterification of natural acids and alcohols. The expected ester yield of the esterification reaction using acetic acid as an acyl donor depends on certain characteristics of the alcohol according to a well-defined tendency. It can be assumed that a similar tendency (though distinct in terms of rate) could be observed for other enzymes regarding the effect of the alcohol. This should be studied separately to decide whether a similar tendency could be detected if various acids are used with the same alcohol.

REFERENCES

[1] Bommarius, A.S.; Riebel, B.R. Biocatalysis (Wiley-VCH Verlag GmbH & Co. KGaA, Weinheim, Germany) 2004 pp. 339-372 DOI: 10.1002/aoc.651

[2] Yan, H-D.; Zhang, Q.; Wang, Z.: Biocatalytic synthesis of short-chain flavor esters with high substrate loading by a whole-cell lipase from *Aspergillus oryzae*, *Catal. Commun.,* 2014 **45**, 59–62 DOI: 10.1016/j.catcom.2013.10.018

[3] Almeida, A.G.; de Meneses, A.C.; de Araújo, P.H.; de Oliveira, D.: A review on enzymatic synthesis of aromatic esters used as flavor ingredients for food, cosmetics and pharmaceuticals industries, *Trends Food Sci. Tech.,* 2017 **69**, 95–105 DOI: 10.1016/j.tifs.2017.09.004

[4] Xu, Y.; Wang, D.; Mu, X.Y.; Zhao, G.A.; Zhang, K.C.: Biosynthesis of ethyl esters of short-chain fatty acids using whole-cell lipase from *Rhizopus chinesis* CCTCC M201021 in non-aqueous phase, *J. Mol. Cat. B-Enzym.,* 2002 **18**, 29–37 DOI: 10.1016/S1381-1177(02)00056-5

[5] Martins, A.B.; Schein, M.F.; Friedrich, J.L.; Fernandez-Lafuente, R.; Ayub, M.A.; Rodrigues, R.C.: Ultrasound-assisted butyl acetate synthesis catalyzed by Novozym 435: Enhanced activity and operational stability, *Ultrason. Sonochem*., 2013 **20**(5), 1155–1160 DOI: 10.1016/j.ultsonch. 2013.01.018

[6] Tomke, P.D.; Rathod, V.K.: Ultrasound assisted lipase catalyzed synthesis of cinnamyl acetate via transesterification reaction in a solvent free medium, *Ultrason. Sonochem.,* 2015 **27**, 241–246 DOI: 10.1016/j.ultsonch.2015.04.022

[7] McGinty, D.; Vitale, D.; Letizia, C.S.; Api, A.M.: Fragrance material review on benzyl acetate, *Food Chem. Toxycol.,* 2012 **50**, S363–S384 DOI: 10.1016/j.fct.2012.02.057

[8] Gubicza, L.; Kabiri-Badr, A.; Keoves, E.; Belafi-Bako, K.: Large-scale enzymatic production of natural flavour esters in organic solvent with continuous water removal, *J. Biotechnol.,* 2000 **84**, 193–196 DOI: 10.1016/S0168-1656(00)00352-7

[9] Doukyu, N.; Ogino, H.: Organic solvent-tolerant enzymes, *Biochem. Eng. J.,* 2010 **48**, 270–282 DOI: 10.1016/j.bej.2009.09.009

[10] de los Ríos, A.P.; Hernández-Fernández, F.J.; Tomás-Alonso, F.; Gómez, D.; Víllora G.: Synthesis of flavour esters using free Candida antarctica lipase B in ionic liquids, *Flavour Frag. J.,* 2008 **23**, 319–322 DOI: 10.1002/ffj.1884

[11] Major, B.; Nemestóthy, N.; Bélafi-Bakó, K.; Gubicza, L.: Enzymatic esterification of lactic acid under microwave conditions in ionic liquids, *Hung. J. Ind. Chem.,* 2008 **36,** 77–81

[12] dos Santos, P.; Meireles, M.A.; Martínez, J.: Production of isoamyl acetate by enzymatic reactions in batch and packed bed reactors with supercritical CO_2, *J. Supercrit. Fluids,* 2017 **127**, 71–80 DOI: 10.1016/j.supflu. 2017.03.019

[13] Sun, J.; Yu, B.; Curran, P.; Liu, S.Q.: Lipase-catalysed ester synthesis in solvent-free oil system: Is it esterification or transesterification?, *Food Chem.,* 2013 **141**, 2828–2832 DOI: 10.1016/j.foodchem.2013.05.109

[14] Csanádi, Z.; Kurdi, R.; Bélafi-Bakó, K.: Ethyl-acetate synthesis in gas phase by immobilized lipase, *Hung. J. Ind. Chem.,* 2012 **40**, 39–44

[15] Findrik, Z.; Nemeth, G.; Vasic-Racki, D.; Belafi-Bako, K.; Csanadi, Z.; Gubicza, L.: Pervaporation-aided enzymatic esterifications in non-conventional media, *Process Biochem*., 2012 **47,** 1715–1722 DOI: 10.1016/j.procbio.2012.08.003

[16] Romero, M.; Calvo, L.,; Alba, C.; Habulin, M.; Primozic, M.; Knez, Z.: Enzymatic synthesis of isoamyl acetate with immobilized *Candida antarctica* lipase in supercritical carbon dioxide, *J. Supercrit. Fluids,* 2005 **33**, 77-84 DOI: 10.1016/j.supflu.2004.05.004

[17] Romero, M.D.; Gómez, J.M.; Díaz-Suelto, B.; García-Sanz, A.: Study of the influence of alcohols in the synthesis of short chain esters, *Chem. Eng. Trans.,* 2011 **24**, 37-42 DOI: 10.3303/CET1124007

[18] Pan, Y.; Tang, K.V.; He, C.; Yi, W.; Zhu, W.; Liu, Y.: Effect of alcohol chain length on the enzymatic resolution of racemic mandelic acid and kinetic study, *Biotechnol. Appl. Biochem.,* 2014 **61**(3), 274-279 DOI: 10.1002/bab.1170

[19] Kumar, R.; Modak, J.; Madras, G.: Effect of chain length of alcohol on the lipase-catalyzed esterification of propionic acid in supercritical carbon dioxide, *Appl. Biochem. Biotechnol.* 2010 **160**, 2342-2354 DOI: 10.1016/j.bej.2005.01.007

[20] Neji, S.B.; Trabelsi, M.; Frikha, M.H.: Esterification of fatty acids with short-chain alcohols over commercial acid clays in a semi-continuous reactor, *Energies,* 2009 **2**, 1107-1117 DOI: 10.3390/en20401107

[21] Stavarache, C.; Vinatoru, M.; Nishimura, R.,; Maeda, Y.: Fatty acids methyl esters from vegetable oil by means of ultrasonic energy, *Ultrason. Sonochem.,* 2005 **12**, 367-372 DOI: 10.1016/j.ultsonch.2004.04.001

[22] Berger, R.G.: Biotechnology as a source of natural volatile flavors, *Curr. Opin. Food Sci.,* 2011 **1**(2), 38–43 DOI: 10.1016/j.cofs.2014.09.003

DE GRUYTER

HUNGARIAN JOURNAL OF INDUSTRY AND CHEMISTRY
Vol. 45(2) pp. 41–44 (2017)
hjic.mk.uni-pannon.hu
DOI: 10.1515/hjic-2017-0019

HUNGARIAN JOURNAL OF INDUSTRY AND CHEMISTRY
HJIC

STATE-OF-THE-ART RECOVERY OF FERMENTATIVE ORGANIC ACIDS BY IONIC LIQUIDS: AN OVERVIEW

KONSTANTZA TONOVA*

Institute of Chemical Engineering, Bulgarian Academy of Sciences, Acad. G. Bonchev Str., Bl. 103, 1113 Sofia, BULGARIA

The main achievements of liquid–liquid extraction (LLE) of fermentative organic acids from their aqueous sources using a diverse range of ionic liquids are summarized since the first study appeared in 2004. The literature survey is organized in consideration of the distinct chemical structures of the organic acids. The acids discussed include mono– or dicarboxylic ones (butyric, L-malic and succinic acids), acids bearing both carboxyl and hydroxyl groups (L-lactic, citric and mevalonic acids), and volatile organic acids (mainly acetic acid). Information is given about ionic liquids applied in recovery, and the resultant extraction efficiencies and partition coefficients. As the topic is novel and experimental studies scarce, the selection of the ionic liquids that were tested still seems random. This may well change in the future, especially after improving the ecological and toxicological characteristics of the ionic liquids in order to bring about an "*in situ*" method of extraction without harming the microbial producers of the organic acids.

Keywords: extraction, ionic liquid, organic acid, recovery, re–extraction

1. Introduction

Room temperature ionic liquids (ILs) exist as molten salts at ambient temperature and consist entirely of ions, usually a charge–stabilized organic cation and an inorganic or organic anion. ILs can be tailored to a wide variety of applications by combining different ions [1] and for this reason they are often called "designer solvents". ILs exhibit a broad range of unique properties, including negligible vapor pressure, high thermal stability and low chemical reactivity [2]. The union of these particular properties, together with finely tunable density, viscosity, polarity and miscibility with other common solvents favor the application of ILs in different kinds of separation and reaction processes [3–8].

Considering the benefits that arise from the properties of ILs, Matsumoto et al. [9] first proposed an environmentally friendly system for the extraction of fermentative L-lactic acid. They used hydrophobic $[C_nC_1im][PF_6]$ instead of volatile organic solvents as diluents of reactive organic bases. These ILs proved to be nontoxic towards the lactic acid producing bacterium *Lactobacillus rhamnosus*, but provided low degrees of solubility of the reactive amines which resulted in insufficient levels of extraction efficiency. Nevertheless, these results suggest possible applications of ILs in extractive fermentations.

*Correspondence: konstantzatonova@yahoo.com

2. Discussion on the organic acids extracted and the ionic liquids applied

2.1. Butyric acid and phosphinate–based ILs

The most remarkable results regarding the partition coefficient of an organic acid in an IL have been documented with regards to the extraction of butyric acid, the four–carbon fatty acid, with phosphinate-based ([Phos]) ILs. $[P_{6,6,6,14}][Phos]$ and a novel ammonium phosphinate, $[C_nC_nC_nC_1N][Phos]$, were studied [10-11]. Distribution coefficients of about 80 were obtained using the low concentrations of butyric acid, and the extraction efficiency was just as high in the pure (water saturated) IL as in the IL/water/dodecane reversed micellar solution. The ammonium phosphinate absorbed a relatively high amount of water until saturation was achieved, *ca* 21 wt%. (about 12 water molecules per ion pair of the IL), which implies that an aqueous biphasic system was formed.

2.2. Dicarboxylic acids and phosphonium- or imidazolium-based ILs

Among phosphonium-based ILs, $[P_{6,6,6,14}]Cl$ seems the most suitable extractant for the recovery of low and moderate concentrations of dicarboxylic L-malic acid in aqueous solutions [12]. The other phosphonium-based ILs and higher acid concentrations entrain third-phase formation, especially in the case of $[P_{6,6,6,14}][Phos]$ when a large amount of the acid content (*ca* 40%) remains

uncovered in both phases. The $[P_{6,6,6,14}]Cl$–rich phase is also the best extractant for another dicarboxylic acid, succinic acid [12]. Extractions with [Dec]- and [Phos]–based ILs resulted in a substantial amount of undetectable acid in both phases, which was attributed to the formation of complexes between the organic acid and the extractants that were not quantified.

More recently succinic acid attracted special attention in a comprehensive study where the extraction was carried out by aqueous biphasic systems (ABS) of alcohols/salts or imidazolium-based ILs/salts [13]. Successful recovery was achieved by both systems. Succinic acid preferentially migrates to the IL–rich phase in all systems formed of $[C_6C_1im]Br$ and a kosmotropic salt (phosphate, sulfate, carbonate or citrate). The IL salted out by $(NH_4)_2SO_4$ or K_2CO_3 exhibited the highest levels of extractability. The pH values of these systems were quite different. The pH of the system with $(NH_4)_2SO_4$ was 3.43 which is below the pK_a values of succinic acid (pK_{a1} = 4.21, pK_{a2} = 5.72), while pH = 10.50 for K_2CO_3 greatly exceeded the pK_a*s*. This suggests that unlike the aqueous biphasic systems with alcohols, the extraction capacity of the IL/salts systems towards succinic acid is not pH–dependent and is most likely related to the proper nature of the solvent (IL/salt) and the solute (acid). For the same IL, $[C_6C_1im]Br$, an excellent solvating capacity to the lactic acid was reported [14] so that the acid could be extracted from a concentrate of white wine. This way the extraction efficiencies of the ABS of $[C_6C_1im]Br/(NH_4)_2SO_4$ or K_2CO_3 are comparable to those obtained with the hydrophobic IL $[P_{6,6,6,14}]Cl$ [12]. Moreover, the re–extraction efficiency achieved was superior at ~71%. Succinic acid was obtained in a crystalline form by direct precipitation with sodium hydroxide.

2.3. Acids with both hydroxyl and carboxyl groups and phosphonium- or imidazolium-based ILs

Different types of phosphonium-based IL biphasic systems were applied for L–lactic acid recovery. An extraction efficiency of above 80% was achieved by using either pure $[P_{6,6,6,14}][Phos]$ [12] or a mixed biphasic system of $[P_{6,6,6,14}]Cl$ and an inorganic kosmotrope, $MgSO_4$ [15]. The kosmotropic salt engages more water molecules when hydrated thus rendering the microenvironment of the acid more hydrophobic which favors the undissociated form of acid suitable for extraction. All extraction systems of phosphonium-based ILs with long side chains suffer from the common disadvantage of forming stable emulsions or a third phase between the IL–rich phase and aqueous solution. This drawback is avoided by applying ILs of an imidazolium cationic moiety, however, in the majority of the cases these ILs exhibit low levels of extraction efficiency towards lactic acid [9,16] and other acids bearing both hydroxyl and carboxyl groups (citric and mevalonic acids) [16].

An advantageous ABS of imidazolium saccharinate, that possesses a long side chain, $[C_{8/10}C_1im][Sac]$, has been exploited lately and it was shown that when it is combined with an inorganic kosmotropic salt (that retains water from solubilization into the IL–rich phase) an extraction efficiency of 81% and partition coefficient of 5.5 could be achieved [17]. The extraction yield of lactic acid was as high as 90% in a two–step recovery by $[C_8C_1im][Sac]$ with or without the addition of a kosmotropic salt ($MgSO_4$). Moreover, successful acid re–extraction of 95% from the IL–rich phase was attained by means of a solution containing an alkaline kosmotrope, K_2HPO_4.

2.4. Volatile fatty acids and phosphonium-based ILs

Apart from culture broths, fermented wastewater streams still represent an unexploited source of platform chemicals, including volatile organic acids. Volatile fatty acids are versatile carboxylic acids involved in the synthesis of bioplastics and other value–added chemicals [18]. The composition of fermented wastewater typically contains ~1 wt% of volatile fatty acids, but also a significant amount of various dissolved salts. The low concentrations of the volatile fatty acids and the large quantity of inorganic salt–originating ions result in pH–values of between 4 and 6, which are in favor of the deprotonated acid form and thus do not support complexation with the IL. The distribution of acetic acid between model solutions with or without salts and different solvents, including phosphonium-based ILs, was recently studied [19]. Similarly to the butyric and lactic acids [10,20], the low concentration of acetic acid and the use of $[P_{6,6,6,14}][Phos]$ were the best conditions to obtain the highest partition coefficient in the IL–rich phase starting from an idealized aqueous solution containing only the acetic acid. In the presence of salts (KCl, Na_2SO_4 or Na_2HPO_4), however, the partition coefficients reported for $[P_{6,6,6,14}]Cl$ were the highest in the series of ILs tested and exceeded even those obtained in the classical extraction by trioctylamine (TOA)/n-octanol. $[P_{6,6,6,14}]Cl$ as a solvent has an inevitable drawback related to its measurable level of leaching into the aqueous phase due to the hydrophilicity of the $[Cl]^-$. Contrary to $[P_{6,6,6,14}]Cl$, $[P_{6,6,6,14}][Phos]$ and $[P_{6,6,6,14}][N(CN)_2]$ were found to be highly stable as significant leaching was not detected in the aqueous phases [19]. Extraction by $[P_{6,6,6,14}][Phos]$, however, was strongly affected by the ions of the salts present in the feed, while $[P_{6,6,6,14}]Cl$ and $[P_{6,6,6,14}][N(CN)_2]$ kept extraction capacities constant for acetic acid. When the source contained different acids, mimicking actual fermented wastewater, it was found that the growing hydrophobic domain in the acid leads to higher degrees of extraction. Butyric acid was the most extracted acid from the fermented wastewater, while lactic acid was the most challenging acid to extract. By modifying the solvent properties of $[P_{6,6,6,14}][Phos]$ by sparging pressurized CO_2, a further increase in the extractability of acetic acid was observed

[21]. The effect was attributed to the altered structure of the fluid which becomes more accessible for the acetic acid. This finding constitutes a general concept for the improvement of extraction processes other than those involving volatile fatty acids.

ILs can act as solvents and simultaneously mediate reactive extraction to valorize low–titer volatile fatty acids. This has been recently shown through an IL–mediated esterification of acetic acid recovered from dilute aqueous streams [22]. The acids produced in anaerobic digestion or fermentation were transferred to a nonvolatile hydrophobic phase where they reacted with an alcohol (ethanol) in order to generate volatile, value–added esters of low solubility. $[P_{6,6,6,14}]$–ILs were selected for their potentially high extracting capacity and hydrophobicity. Their hydrophobic character provides a water-excluding site for esterification and a nonvolatile carrier for the evaporation of the ester produced. Significant accumulation of acetic acid in the IL was achieved by using $[P_{6,6,6,14}][N(CN)_2]$, but this was mainly due to the exchange of $[N(CN)_2]^-$ for the acetate anion as the dicyanamide anion was found to hydrolyze under the extraction conditions used, including at an elevated temperature (75 °C). Contrary to the extraction, $[P_{6,6,6,14}][N(CN)_2]$ and $[P_{6,6,6,14}]Cl$ appeared to be the worst media for performing esterification, while the best was $[P_{6,6,6,14}][Tf_2N]$, which, however, is poor and costly extractant. Thus an IL of combined anions, $Cl^- + [Tf_2N]^-$, was tested which could be used in a multistage way. Starting from an aqueous stream of 0.33 mol dm^{-3} acetic acid, 0.44 mol dm^{-3} accumulated in the mixed $[P_{6,6,6,14}]Cl+[Tf_2N]$ which allowed an esterification conversion of 56% to be achieved over 30 min.

3. Conclusion

ILs are commonly considered more sustainable than classical organic solvents. It is well known that the toxicity level of conventional solvents to microbes limits their compatibility with fermentation broths. However, the label of "green solvent", assigned to the ILs, has led to the delusion that they are nontoxic and biodegradable, which is not true about some of the most employed ILs. For example, the commonly used $[P_{6,6,6,14}]Cl$ may be regarded as toxic in aquatic environments exhibiting much higher levels of ecotoxicity compared to ordinary organic solvents [23]. The biocompetitiveness and biodegradability of ILs are not still convincingly argued for [24-25]. The need for novel extractants with improved characteristics from ecological and toxicological standpoints can be put forward. By taking into account that aqueous streams and bioorganics are treated, the environmental impact of ILs should be resolved as a result of future studies.

SYMBOLS

IL's cationic moiety:
$[C_nC_1im]$ 1-alkyl-3-methylimidazolium
$[C_nC_nC_nC_1N]$ trialkylmethylammonium
$[P_{6,6,6,14}]$ tetradecyl(trihexyl)phosphonium
IL's anionic moiety:
[Dec] decanoate
$[N(CN)_2]$ dicyanamide
[Phos] bis(2,4,4-trimethylpentyl)phosphinate
[Sac] saccharinate (which is a benzoic sulfimide)
$[Tf_2N]$ bis(trifluoromethylsulfonyl)imide
Other:
TOA trioctylamine

Acknowledgement

This research was supported by the Bulgarian Science Fund (Contract grant DFNI–B01/23).

REFERENCES

[1] Blundell, R.K.; Licence, P.: Quaternary ammonium and phosphonium based ionic liquids: A comparison of common anions, *Phys. Chem. Chem. Phys.*, 2014 **16**(29), 15278–15288 DOI: 10.1039/C4CP01901F

[2] Freemantle, M.: An Introduction to Ionic Liquids (RSC Publishing, Cambridge, UK) 2009

[3] Mutelet, F.; Jaubert, J.-N.: Interactions between organic compounds and ionic liquids. Selectivity and capacity characteristics of ionic liquids, Chapter 10 in *Ionic Liquids: Theory, Properties, New Approaches*, Ed.: Kokorin, A. (InTech) 2011 DOI: 10.5772/14291

[4] Tonova, K.: Separation of poly- and disaccharides by biphasic systems based on ionic liquids, *Sep. Purif. Technol.*, 2012 **89**, 57–65 DOI: 10.1016/j.seppur.2012.01.007

[5] Keremedchieva, R.; Svinyarov, I.; Bogdanov, M.G.: Ionic liquid–based aqueous biphasic systems – A facile approach for ionic liquid regeneration from crude plant extracts, *Processes*, 2015 **3**(4), 769–778 DOI: 10.3390/pr3040769

[6] Tonova, K.; Bogdanov, M.G.: Partitioning of α-amylase in aqueous biphasic system based on hydrophobic and polar ionic liquid: Enzyme extraction, stripping and purification, *Sep. Sci. Technol.*, 2017 **52**(5), 812–823 DOI: 10.1080/01496395.2016.1267211

[7] Fehér, E.; Illeová, V.; Kelemen-Horváth, I.; Bélafi-Bakó, K.; Polakovič, M.; Gubicza, L.: Enzymatic production of isoamyl acetate in an ionic liquid–alcohol biphasic system, *J. Mol. Catal. B: Enz.*, 2008 **50**(1), 28–32 DOI: 10.1016/j.molcatb.2007.09.019

[8] Major, B.; Nemestóthy, N.; Bélafi-Bakó, K.; Gubicza, L.: Enzymatic esterification of lactic acid under microwave conditions in ionic liquids, *Hung. J. Ind. Chem.*, 2008 **36**(1-2), 77–81

[9] Matsumoto, M.; Mochiduki, K.; Fukunishi, K.; Kondo, K.: Extraction of organic acids using imid-imidazolium–based ionic liquids and their toxicity to *Lactobacillus rhamnosus*, *Sep. Purif. Technol.*, 2004 **40**(1), 97–101 DOI: 10.1016/j.seppur.2004.01.009

[10] Marták, J.; Schlosser, Š.: Liquid–liquid equilibria of butyric acid for solvents containing a phosphonium ionic liquid, *Chem. Pap.*, 2008 **62**(1), 42–50 DOI: 10.2478/s11696-007-0077-5

[11] Blahušiak, M.; Schlosser, Š.; Marták, J.: Extraction of butyric acid with a solvent containing ammonium ionic liquid, *Sep. Purif. Technol.*, 2013 **119**, 102–111 DOI: 10.1016/j.seppur.2013.09.005

[12] Oliveira, F.S.; Araújo, J.M.M.; Ferreira, R.; Rebelo, L.P.N.; Marrucho, I.M.: Extraction of L-lactic, L-malic, and succinic acids using phosphonium–based ionic liquids, *Sep. Purif. Technol.*, 2012 **85**, 137–146 DOI: 10.1016/j.seppur.2011.10.002

[13] Pratiwi, A.I.; Yokouchi, T.; Matsumoto, M.; Kondo, K.: Extraction of succinic acid by aqueous two–phase system using alcohols/salts and ionic liquids/salts, *Sep. Purif. Technol.*, 2015 **155**, 127–132 DOI: 10.1016/j.seppur.2015.07.039

[14] Lateef, H.; Gooding, A.; Grimes, S.: Use of 1-hexyl-3-methylimidazolium bromide ionic liquid in the recovery of lactic acid from wine, *J. Chem. Technol. Biotechnol.*, 2012 **87**(8), 1066–1073 DOI: 10.1002/jctb.3843

[15] Tonova, K.; Svinyarov, I.; Bogdanov, M.G.: Biocompatible ionic liquids in liquid–liquid extraction of lactic acid: A comparative study, *Int. J. Chem. Nuclear Mater. Metallurgical Eng.*, 2015 **9**(4), 526–530 https://www.waset.org/publications/10001024

[16] Li, Q.Z.; Jiang, X.L.; Zou, H.B.; Cao, Z.F.; Zhang, H.B.; Xian, M.: Extraction of short–chain organic acids using imidazolium–based ionic liquids from aqueous media, *J. Chem. Pharm. Res.*, 2014 **6**(5), 374–381 http://www.jocpr.com/articles/extraction-of-shortchain-organic-acids-using-imidazoliumbased-ionic-liquids-from-aqueous-media.pdf

[17] Tonova, K.; Svinyarov, I.; Bogdanov, M.G.: Hydrophobic 3-alkyl-1-methylimidazolium saccharinates as extractants for L-lactic acid recovery, *Sep. Purif. Technol.*, 2014 **125**, 239–246 DOI: 10.1016/j.seppur.2014.02.001

[18] Straathof, A.J.J.: Transformation of biomass into commodity chemicals using enzymes or cells, *Chem. Rev.*, 2014 **114**(3), 1871–1908 DOI: 10.1021/cr400309c

[19] Reyhanitash, E.; Zaalberg, B.; Kersten, S.R.A.; Schuur, B.: Extraction of volatile fatty acids from fermented wastewater, *Sep. Purif. Technol.*, 2016 **161**, 61–68 DOI: 10.1016/j.seppur.2016.01.037

[20] Marták, J.; Schlosser, Š.: Extraction of lactic acid by phosphonium ionic liquids, *Sep. Purif. Technol.*, 2007 **57**, 483–494 DOI: 10.1016/j.seppur.2006.09.013

[21] Reyhanitash, E.; Zaalberg, B.; Ijmker, H.M.; Kersten, S.R.A.; Schuur, B.: CO_2–enhanced extraction of acetic acid from fermented wastewater, *Green Chem.*, 2015 **17**(8), 4393–4400 DOI: 10.1039/C5GC01061F

[22] Andersen, S.J.; Berton, J.K.E.T.; Naert, P.; Gildemyn, S.; Rabaey, K.; Stevens, C.V.: Extraction and esterification of low–titer short–chain volatile fatty acids from anaerobic fermentation with ionic liquids, *Chem. Sus. Chem.*, 2016 **9**(16), 2059–2063 DOI: 10.1002/cssc.201600473

[23] Wells, A.S.; Coombe, V.T.: On the freshwater ecotoxicity and biodegradation properties of some common ionic liquids, *Org. Process Res. Dev.*, 2006 **10**(4), 794–798 DOI: 10.1021/op060048i

[24] Siedlecka, E.M.; Czerwicka, M.; Neumann, J.; Stepnowski, P.; Fernández, J.F.; Thöming, J.: Ionic liquids: Methods of degradation and recovery, Chapter 28 in *Ionic Liquids: Theory, Properties, New Approaches*, Ed.: Kokorin, A. (InTech) 2011 DOI: 10.5772/15463

[25] Egorova, K.S.; Ananikov, V.P.: Toxicity of ionic liquids: Eco(cyto)activity as complicated, but unavoidable parameter for task–specific optimization, *Chem. Sus. Chem.*, 2014 **7**(2), 336–360 DOI: 10.1002/cssc.201300459

DE GRUYTER

HUNGARIAN JOURNAL OF
INDUSTRY AND CHEMISTRY
Vol. 45(2) pp. 45–49 (2017)
hjic.mk.uni-pannon.hu
DOI: 10.1515/hjic-2017-0020

HUNGARIAN JOURNAL OF INDUSTRY AND CHEMISTRY
HJIC

APPLICATION OF A HYDROPHOBIC POLYMERIC MEMBRANE FOR CARBON DIOXIDE DESORPTION FROM AN MEA-WATER SOLUTION

ZENON ZIOBROWSKI*, ADAM ROTKEGEL

Institute of Chemical Engineering of the Polish Academy of Sciences, ul. Balycka 5, 44-100 Gliwice, POLAND

Carbon dioxide desorption from a monoethanolamine (MEA) solution using a hydrophobic polydimethylsiloxane (PDMS) tubular membrane on a ceramic support is presented. The effects of operating parameters such as feed temperature, liquid flow rate and MEA concentration on mass transfer were examined. The mass transfer of CO_2 from the liquid to gaseous phase was predicted by a multilayer film model with an accuracy of ±25%. Research into new selective materials is needed to develop more efficient and environmentally friendly CO_2 capture technology

Keywords: MEA, desorption, carbon dioxide, hydrophobic membrane, PDMS

1. Introduction

Fossil fuel combustion from power plants is one of the most significant sources of CO_2 emissions [1]. The separation of carbon dioxide from gases can be realized by processes such as adsorption, absorption, low temperature distillation and membrane separation. The absorption of carbon dioxide in amine based solutions is currently the most widespread method in industry for the post-combustion capture of CO_2 [2].

The advantage of chemical absorption in amine solutions is the fact that at higher temperatures the chemical reaction can be reversed and the amine recycled. On the other hand, obstacles include a relatively low CO_2 capture capacity, solvent losses caused by evaporation, thermal stability, highly corrosive characteristics, ecotoxicity and biodegradability in the natural environment [2-4]. It was shown that MEA and diethanolamine (DEA) might promote potential long-term toxicity effects towards living organisms [5,6]. In addition the regeneration step may increase the total operating costs of the capture plant by up to 70%, especially for primary and tertiary amines where the heat of reaction is quite high [7].

The amine scrubbing processes carried out in packed columns are currently most widely used in industry for the post-combustion capture of CO_2. Limiting factors for the application of this technology are its size and large capital costs. The mass transfer performance of this solution can be reduced by flooding, foaming and entrainment conditions.

*Correspondence: zenz@iich.gliwice.pl

In comparison to the studies on CO_2 absorption in MEA solutions there are only a few concerning CO_2 desorption, despite the fact that the stripping unit is responsible for most of the separation cost of the process [8].

It is important that materials used in the processes concerning post-combustion capture of CO_2 exhibit low or no environmental effects. Various tubular membranes were operated as catalyst supports [9]. Recently a new type of ceramic hollow fiber membrane contactor has been studied [10]. This kind of membrane can be modified to be hydrophobic which enables it to be applied for CO_2 absorption-desorption in amine solutions. In this study the process of CO_2 removal from an MEA solution using a hydrophobic polydimethylsiloxane (PDMS) tubular membrane on a ceramic support was investigated.

2. Experimental

2.1. Experimental setup

The experimental setup shown in *Fig.1* consisted of a membrane module, reactor vessel, cooling system, as well as circulation and vacuum pumps. The hydrophobic PDMS membranes on ceramic support (ceramic tubes with an outer diameter of 0.01 m and length of 0.25 m using a PVM 250 membrane module made by Pervatech BV) was studied.

The feed was circulated by a pump and the flow rate was controlled by a flowmeter. In all experiments the feed temperature was stabilized by a thermostat (±1°C). The permeate was condensed and collected in cold traps immersed in liquid nitrogen. The vacuum pump was used to maintain the pressure between 7 and 10 mmHg on the permeate side. The concentration of

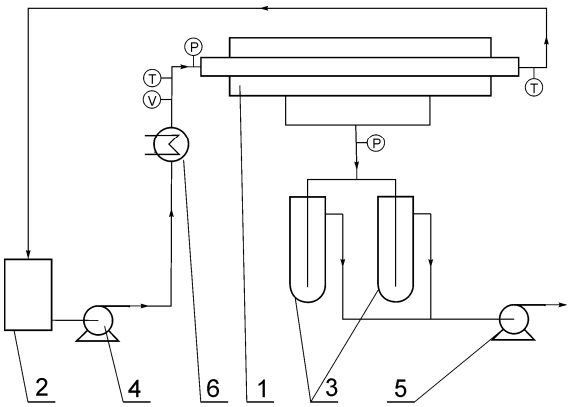

Figure 1. The experimental setup: 1 – membrane contactor, 2 – feed tank, 3 – cold traps, 4 – circulation pump, 5 – vacuum pump, 6 – heater

carbon dioxide in the permeate was calculated by measuring the mass of carbon dioxide and water in the analyzed permeate sample. The pressures on the feed and permeate sides were measured by pressure gauges. The temperatures of the feed in the reactor vessel, before and after the membrane module were measured by thermocouples.

Pure monoethanolamine (MEA) and deionised water were used to prepare the liquid-feed solution. Afterwards the obtained solution was loaded with CO_2 by bubbling pure CO_2 in a magnetically stirred vessel until the required carbonation ratio, α, was achieved. In our experiments the carbonation ratio was determined by measuring the mass of absorbed CO_2 in the amine solution at a given temperature.

Additionally, independent pervaporation experiments with the same PDMS membrane under similar thermal and hydrodynamic conditions for a 2-propanol – water mixture were performed to estimate the membrane resistance ($1/k_M$).

2.2. Experimental results

The performance of the PDMS membrane was examined experimentally. The operating temperature was between 323 and 348K (50 and 75°C), liquid flow rate between 20 and 600 l/h and the MEA concentrations were 5, 10 and 15 wt%.

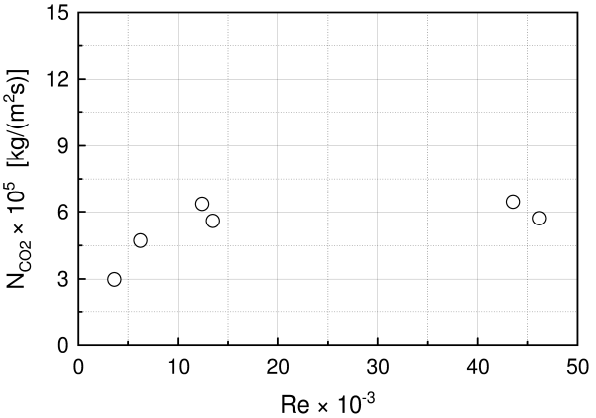

Figure 2. The effect of Re number on CO_2 mass flux (T = 50°C, w_{MEA} = 10 wt%)

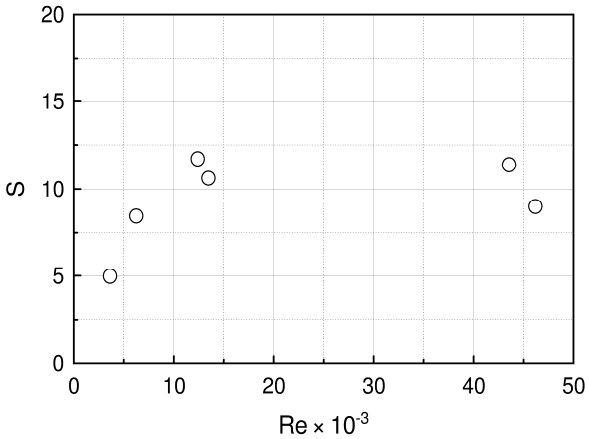

Figure 3. The effect of Re number on selectivity (T = 50°C and w_{MEA} = 10 wt%)

The effect of liquid flow rate on the CO_2 mass flux and selectivity is presented in *Figs.2* and *3* for the temperature of 323K (50°C) and 10% MEA concentration. The selectivity of the process is defined as follows:

$$S = \frac{(w_{CO_2}(1-w_{CO_2}))_p}{(w_{CO_2}(1-w_{CO_2}))_f} \quad (1)$$

The measured fluxes increase with the Reynolds number. The highest values were obtained for Re>10,000 (turbulent flow). This can be explained by the CO_2 mass transfer increase in the liquid phase for turbulent regime. The measured selectivities rise with the Reynolds number and for turbulent flows reach the value of 10.

The operating temperature is an important parameter as far as the efficiency of the membrane is concerned as shown in *Fig.4*. For a given turbulent liquid flow rate the measured CO_2 mass fluxes rise with the feed temperatures due to the increased driving force in favour of CO_2 mass transfer. The selectivity does not change significantly with the operating temperature, *Fig.5*.

The effect of the MEA concentration on mass flux and selectivity is presented in *Figs.6-7* at an operating temperature of 323K (50°C) and turbulent flow (Re of about 40,000).

The measured mass fluxes do not change significantly with MEA concentration (*Fig.6*), because of the

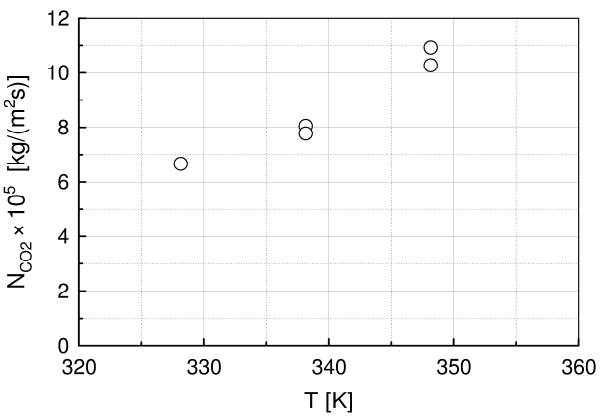

Figure 4. The effect of feed temperature on CO_2 mass flux (w_{MEA} = 10 wt%)

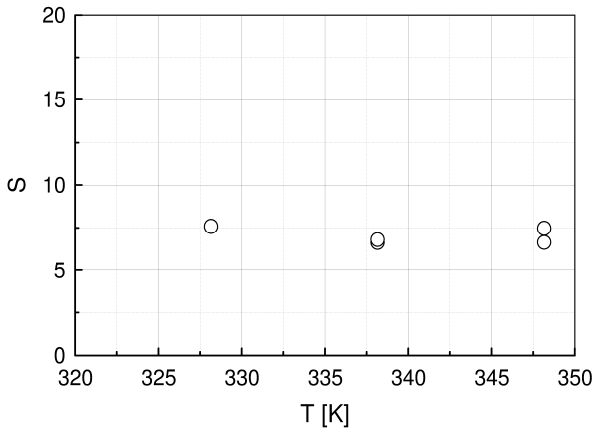

Figure 5. The effect of feed temperature on selectivity (w_{MEA} = 10 wt%)

relationship between equilibrium constants of the CO_2 - MEA reaction and the CO_2 solubility in water at a given temperature. The selectivity decreases with MEA concentration as a result of the rising amount of CO_2 absorbed in the MEA solution and the constant CO_2 flux in the permeate, see *Fig.7*.

3. Mathematical model and calculation results

When CO_2 is absorbed in aqueous monoethanolamine (MEA) solution, the following reactions can be written as [11]:

$$CO_2 + RNH_2 \xrightarrow{\text{slow}} RN^+H_2COO^- \quad (2)$$

$$RN^+H_2COO^- + RNH_2 \xrightarrow{\text{fast}} RNH_3^+ + RNHCOO^- \quad (3)$$

The formation of carbamate is well understood and the rate of the forward reaction has been determined as first order with respect to both CO_2 and RNH_2:

$$r = k_{CF}[CO_2][RNH_2] \quad (4)$$

During the desorption process the differences in the concentration of the component and the temperature between the inlet and outlet in the liquid phase are very small. Therefore, the desorption rate may be simply calculated using the arithmetic mean value of CO_2 in the liquid phase.

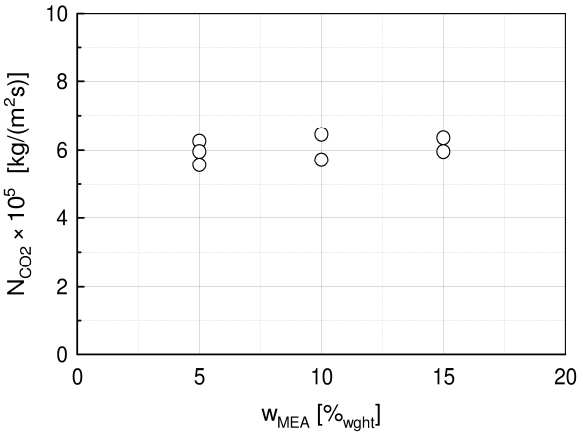

Figure 6. The effect of MEA concentration on CO_2 mass flux

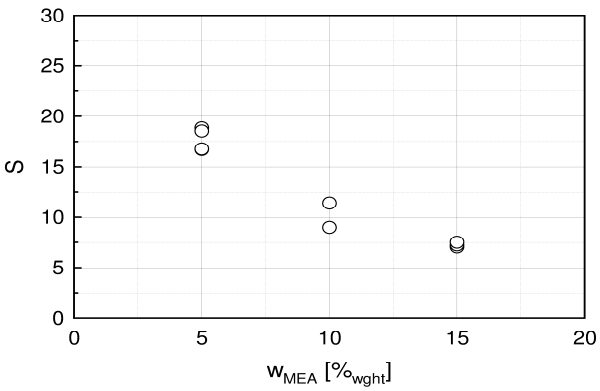

Figure 7. The effect of MEA concentration on selectivity

With this assumption we can calculate the mass fluxes of CO_2 can be calculated as follows:

$$N_{CO_2} = K_L(x_{CO_2} - x^*_{CO_2}) \quad (5)$$

where N_{CO2} [kmol/s] is the flux of CO_2 and K_L [kmol/m^{2}s] is the overall mass-transfer coefficient of the liquid phase.

The overall mass-transfer coefficient for CO_2 can be evaluated by a resistance-in-series model [12].

The numerical calculations based on model equations were performed and estimated values of membrane resistance ($1/k_M$) used. In the calculations the experimental values of the Henry's constant for CO_2 in water and MEA under standard conditions are 1.2456 and 1.5732, respectively [13]. The enhancement factor of the chemical reaction of CO_2 in the liquid phase, as defined by DeCoursey [14], was between 20 and 60. The viscosity of the water–MEA mixture was calculated according to a Grunberg and Nissan equation [15]. Calculated and experimental values of CO_2 mass fluxes are

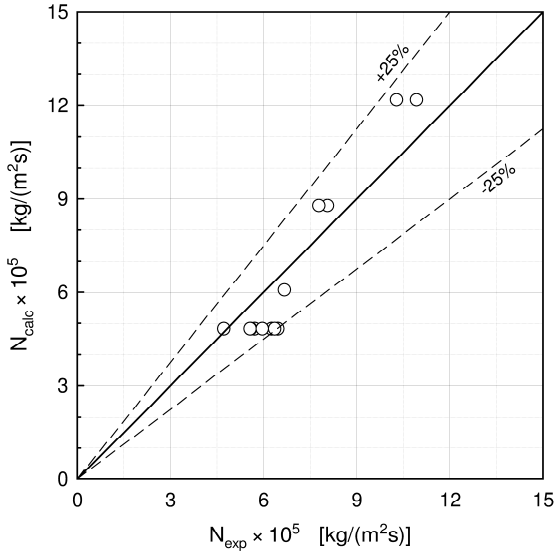

Figure 8. Comparison of calculated values of CO_2 fluxes with experimental ones

shown in *Fig.8*. The scattering of calculated and experimental values of CO_2 mass fluxes was within the range of ±25% .

The experimental values of CO_2 mass fluxes were compared with those obtained from the literature for CO_2 stripping in a ceramic hollow fiber membrane contactor [10]. In spite of the different types of membrane type and hydrodynamic conditions the measured values of CO_2 mass fluxes were comparable in both cases.

Conclusions

The application of a membrane in the process of CO_2 stripping from MEA solutions avoids some technical problems that are encountered in industrial practices.

The PDMS hydrophobic tubular membrane on a ceramic support can be applied for the removal of CO_2 from MEA solutions. In developed turbulent flows the measured CO_2 mass fluxes and selectivities do not change significantly with Re number (*Figs.2-3*). The measured CO_2 mass fluxes increase as the feed temperature rises (*Fig.4*) and slightly depend on the MEA concentration (*Fig.6*). The measured and calculated CO_2 mass fluxes are in good agreement with each other (*Fig.8*). The ±25% variation in scattering can be explained by the accuracy of the correlations, experimental precision and simplification of the model.

4. SYMBOLS

C – concentration, kmol m^{-3}
D – diffusion coefficient, m^2 s^{-1}
K_L – overall mass transfer coefficient, kmol m^{-2} s^{-1}
k_M – mass transfer coefficient of the membrane, kmol m^{-2} s^{-1}
N – mass flux kmol $m^{-2}s^{-1}$
r – reaction rate, kmol s^{-1}
Re – Reynolds number
S – selectivity
T – temperature, K
w – mass fraction
x – mole fraction of CO_2 in the liquid phase

superscripts
* - refers to equilibrium
subscripts
calc – calculation
CO_2 – carbon dioxide
exp - experimental
f – feed
G – gaseous phase
L – liquid phase
p - permeate

REFERENCES

[1] Budzianowski W.M.: Single solvents, solvent blends, and advanced solvent systems in CO_2 capture by absorption: a review, *Int. J. Global Warming*, 2015 **7** (2), 184-225, DOI: 10.1504/IJGW.2015.067749

[2] Rochelle G.T.: Amine scrubbing for CO_2 capture, *Science*, 2009 **325**, 1652-1654, DOI: 10.1126/science.1176731

[3] Zhao B.; Sun Y.; Yuan Y.; Gao J.; Wang S.; Zhuo Y.; Chen C.: Study on corrosion in CO_2 chemical absorption process using amine solution, *Energy Procedia,* 2011 **4**, 93–100, DOI: 10.1016/j.egypro.2011.01.028

[4] Eide-Haugmo I. et al.: Environmental impact of amines, *Energy Procedia* 2009 **1**, 1297–1304, DOI: 10.1016/j.egypro.2009.01.170

[5] Libralato G.; Volpi Ghirardini A.; Avezzù F.: Seawater ecotoxicity of monoethanolamine, diethanolamine and triethanolamine, *J. Hazard. Mat.*, 2010 **176**, 535–539, DOI: 10.1016/j.jhazmat.2009.11.062

[6] Ethanolamine Compounds (MEA, DEA, TEA And Others), online: http://www.safecosmetics.org/get-the-facts/chemicals-of-concern/ethanolamine-compounds/, accessed: 2017-10-05

[7] Schäfer B.; Mather A.E.; Marsh K.N.: Enthalpies of solution of carbon dioxide in mixed solvents, *Fluid Phase Equilib.*, 2002 **194**, 929-935, DOI: 10.1016/S0378-3812(01)00722-1

[8] Dugas R.; Rochelle G.: Absorption and desorption rates of carbon dioxide with monoethanolamine and piperazine, *Energy Procedia*, 2009 **1**, 1163-1169, DOI: 10.1016/j.egypro.2009.01.153

[9] Keil F. J.; Flügge U.: High Performance Catalytic Tubular Membrane Reactors Owing to Forced Convective Flow Operation, *Hung. J. Ind. Chem.,*2005, **32(1-2)**, 31-42

[10] Koonaphapdeelert S.; Wu Z.; Li K.: Carbon dioxide stripping in ceramic hollow fibre membrane contactors, *Chem. Eng. Sci.*, 2009 **64**, 1-8, DOI: 10.1016/j.ces.2008.09.010

[11] Astarita G.; Savage D.W.; Bisio A.: Gas treating with chemical reaction, John Wiley & Sons, New York, 1983

[12] Kreulen H.; Smolders C.A.; Versteeg G.F.; Van Swaaij W.P.M.: Microporous hollow fiber membrane module as gas-liquid contactors. Part 2: Mass transfer with chemical reaction, *J. Membrane Sci.*, 1993 **78**, 217-238, DOI: 10.1016/0376-7388(93)80002-F

[13] Browning G.J.; Weiland R.H.: Physical solubility of carbon dioxide in aqueous alkanolamine via nitrous oxide analogy, *J. Chem. Eng. Data*, 1994 **39**, 817-822, DOI: 10.1021/je00016a040

[14] DeCoursey W.J.: Enhancement factors for gas absorption with reversible reaction, *Chem. Eng. Sci.*, 1982 **37**, 1483-1489, DOI: 10.1016/0009-2509(82)80005-5

[15] Meng-Hui L., Yei-Chung L.: Densities and Viscosities of Solutions of Monoethanolamine + N-Methyldiethanolamine + Water and Monoethanolamine + 2-Amino-2-methyl-1-propanol + Water, J. *Chem. Eng. Data*, 1994 **39**, 444-447, DOI: 10.1021/je00015a009